ADDIS ABABA UNIVERSITY
SCHOOL OF GRADUATE STUDIES

GRAVITY AND ELECTRICAL METHODS FOR GROUNDWATER RESOURES POTENTIAL ASSESEMENT AND MAPPING OF AQUFIERS, WOBOK-DILO AREA, BORENA, SOUTH ETHIOPIA

BY

ABDISA KAWO KOJI

OCTOBER, 2011

ADDIS ABABA

GRAVITY AND ELECTRICAL METHODS FOR GROUNDWATER RESOURES POTENTIAL ASSESEMENT AND MAPPING OF AQUFIERS, WOBOK-DILO AREA, BORENA, SOUTH ETHIOPIA

BY

ABDISA KAWO KOJI

A THESIS SUBMITTED TO THE SCHOOL OF GRADUATE STUDIES OF THE ADDIS ABABA UNIVERSITY IN PARTIAL FULFILLMENT OF THE REQUIREMENTS FOR THE DEGREE OF MASTERS OF SCIENCE IN EXPLORATION GEOPHYSICS

DEPARTMENT OF EARTH SCIENCES

ADDIS ABABA UNIVERSITY

OCTOBER- 2011

ADDIS ABABA

ADDIS ABABA UNIVERSITY

SCHOOL OF GRADUATE STUDIES

GRAVITY AND ELECTRICAL METHODS FOR GROUNDWATER RESOURES POTENTIAL ASSESEMENT AND MAPPING OF AQUFIERS, WOBOK-DILO AREA, BORENA, SOUTH ETHIOPIA

BY

ABDISA KAWO KOJI

(DEPARTMENT OF EARTH SCIENCES)

Approved by board of examiners:

Dr.Tigistu Haile Signature _____

Chairman, Department of

Earth sciences

Dr. Elias Lewi Signature _____

Advisor

Dr. Tigistu Haile Signature _____

Co-Adviser

Dr._____ Signature _____

Internal Examiner

Dr. _____ Signature _____

Examiner

ACKNOWLEDGMENTS

First of all, I would like to thank the almighty God for ever thing He does in my life.

I have got no words to express my adviser Dr. Elias Lewi for his crucial comments and sound suggestions that he gave me in order to accomplish this thesis successfully .During the time that I engaged in this work, he acted like not only my adviser but also like my father and colleague .I thank you for everything that you did for me.

I would like to express my grateful thanks to my co-adviser Dr.Tigistu Haile for his unreserved supports, suggestions and crucial comments to accomplish this work successfully .I have great respect to you because as chair person of the department you seriously look my case and allowed me to readmitted to the programme.

I would like to say great thanks for Dr. Shimeles Fisseha who gave me valuable references, resistivity data, geological report of the study area and unreserved moral and psychological support.

Especial thanks go to my friend Tadele Geleshe and to my brothers Temame Kawo and Mutahar kawo for their unreserved financial and moral support.

My thanks go also to my friends Solomon Sahila, Fantahun Gebre and Berket for their support to use different softwares to process the geophysical data.

Last but not the least, I thank all my families and friends who asked and helped me during the time, when I was in trouble.

ABSTRACT

A combined geophysical survey using vertical electrical sounding (VES) and gravity methods was conducted to investigate groundwater potential zones and geological structures at Wobok-Dilo area, Borena zone, in South Ethiopia. The area being dominantly of basement rock lithology with interspersed volcanics and with scarcely known groundwater potential, the main objectives of this study were to map groundwater potential zones and determine depth to the basement.

Geologically, the Wobok-Dilo area lies on dominantly volcanic terrain. The exposed basaltic formations over the area are highly vesicular and scoracious basalts. The geophysical surveys included twenty one (21) VES points, using Schlumberger electrode array ,with maximum half current electrode spacing AB/2=1000m and 103 gravity measuring points. These were interpreted both qualitatively and quantitatively in order to infer the subsurface geology and identify aquifer bearing horizons.

The qualitative analysis of VES data were performed by using pseudodepth sections and different apparent resistivity maps. Similarly, the qualitative interpretations of gravity data were performed by using different gravity anomaly maps. The quantitative interpretations of the VES data were conducted by modeling the VES data using ResixIP and WinResist modeling software and constructing geoelectric sections along selected survey lines, using the result from individual VES point interpretations. The depth and lithologic units from the borehole was used to constrain the parameters during the modeling of VES data. The information from the VES data and the borehole were also used to constrain the depth information in the gravity modeling which were conducted on one survey line. The VES results revealed six to seven main geoelectric layers which differ in degree of weathering, fracturing, composition and depth of burial. The geoelectric sections enabled to identify the depth to the aquifer along survey lines whereas the gravity model helped to identify basement undulation and map structures. Finally, the overall interpretation was done by integrating all the above results together with the topographic maps and borehole information. As a result of these, geologic structures and groundwater potential zones are identified and drilling sites for potentially productive boreholes are recommended.

TABLE OF CONTENTS **PAGES**

LIST OF FIGURES **PAGE**

LIST OF TABLES

PAGE

ACRONYMS

1D-One Dimension
2D-Two Dimension
3D-Three Dimension
AWD-Acute Water Diarrheal
GRS-Geodetic References System
IGSN-International Gravity Standardization Net
ITRF-International Terrestrial References Frame
IUGG- International Union of Geodesy and Geophysics
MDG- Millennium Development Goal
OWWDSE-Oromia Water Works Design and Supervision enterprise
RMS-Root Mean Square
SWL-Static Water Level
UAP- Universal Access Programme
UTM-Universal Transverse Mercator
UNDP- United Nation Development Program
VES-Vertical Electrical Sounding
WDBH1-Wobok-Dilo Bore Hole one
WGS-World Geodetic System
WHO-World Health Organization
WSDP-Water Sector Development Program

CHAPTER 1

INTRODUCTION

1.1General

Ethiopia is blessed with comparatively large resource of groundwater which provides a replenish able and pollution free natural water resource that is clean through the natural process of purification while passing through geologic formation .In fact, it constitutes the largest available source of fresh water, far greater than those in lakes, reservoirs and streams combine, that is suitable for domestic, agricultural and livestock consumptions (WSDP, 2010). Owing to large resources of fresh (underground) water a large portion of rural Ethiopia is in desperate search for adequate and clean water supply, where in these area problems mainly associated with unavailability of clean water.

According to the reports of Ethiopia Water Bureau (WSDP, 2010) the percentage of clean water access is currently 47% of the total population. The health of about 40 million citizen is exposed to various type of water borne and related diseases which cause high mortality and morbidity rates.

In Ethiopia, endemic (non-out break) diarrheal diseases cause 17% of death in children under 5 years of age and the fourth leading cause of all deaths (Capital News paper Hider 2008 Pp8). Out breaks of acute water diarrheal (AWD) add to the disease burden and require costly diversion of scarce health and other resources to minimize fatalities. Moreover, the diseases associated with contaminated water also exert a heavy economic load on the country, both on public health care for treatments and on persons affected to transport to clinics and provide medicines, which are normally bought with foreign currency and ultimately result in lower productivity of the population.

Water is a precious natural resource- vital for life, national development, and the environment. In too great a quantity or too little, it can bring destruction, misery, or death. Irrespective of how it

occurs, if properly managed, it can be an instrument for economic survival and growth. It can be an instrument to help reduce poverty, lift people out of the degradation of not having enough for their household needs and their livestock. However, when inadequate in quantity and quality, it can hinder the effort in poverty reduction and national development, resulting in poor health and low productivity, food insecurity, and constrained economic development. when its quality is not protected, it can pose serious environmental health risks and adversely affect agricultural and livestock production.

In Ethiopia, like anywhere else, the remotest area like Wobok-Dilo in Borena area of South Ethiopia which is the area of study presented in this work, is the most vulnerable and frequently affected, since they rely essentially on land and water resources to sustain their livelihoods. The productivity of water in agriculture remains generally low in Ethiopia, hampering efforts at income generation, economic growth and sustainable development. The water scarcity affects the women and girls most who have to walk long distance in search of minimal household needs.

As part of the Millennium Development Goal (MDG) the United Nation expressed its commitment by 2015 to reduce by half the 1.1 billion people without access to safe drink water (Capital News paper Hider 2008 pp8). Based on MDG, the Ethiopian government embarked up on implementation of Universal Access Programme (UAP) for safe water supply services designed to radically alter the low coverage and to fully extend these service to all communities in the year 2015. Therefore, the Wobak-Dilo ground water exploration project is among the biggest project that the government of Ethiopia designed both for the implementation of UAP as well as MDG. Furthermore, the people who live in the study area are mainly pastoralist except those found in near towns such as Yabelo, Mega, Dubuluk and Teltle. The pastoralist in the rural area travel from place to place to look for water and pasture for their cattle. Though the availability of constant water supply is one of the major issues that dictate the settlement of the pastoralist in the area, it is not enough by itself for constant settlement due to the demand for enough pasture. Therefore, the detailed geophysical study for groundwater exploration was crucial to assist the effort in ground water exploration.

1.2 Location and Accessibility of the study area

Wobok-Dilo is located in the southwestern part of the Borena Zone, Oromia national regional state, South Ethiopia. It is part of the area of the Borena pastoral regions located to the west of Yabello-Moyale main road along the Ethio-Kenyan boarder in the Dire woreda. The study area is bounded by the longitude-latitude coordinates 37.54088W-37.657516 E, 4.425147S-4.4941N with height variation within the range of 919.207-989.736 from the WGS84 reference ellipsoid. The study area can be reached through two alternative main access roads. The first one is to travel along the asphalt road from Addis Ababa to the town of Moyale via towns of Hawasa, Dilla and zonal town Yabello or Addis Ababa to Arba-Minch, Yabello and finally to Wobok-Dilo. Infrastructure facilities like electricity, telephone, banking, health sector and postal services are not available in the study area, so one needs to travel to Zonal town, Yabello in order to access the above mentioned infrastructural facilities.

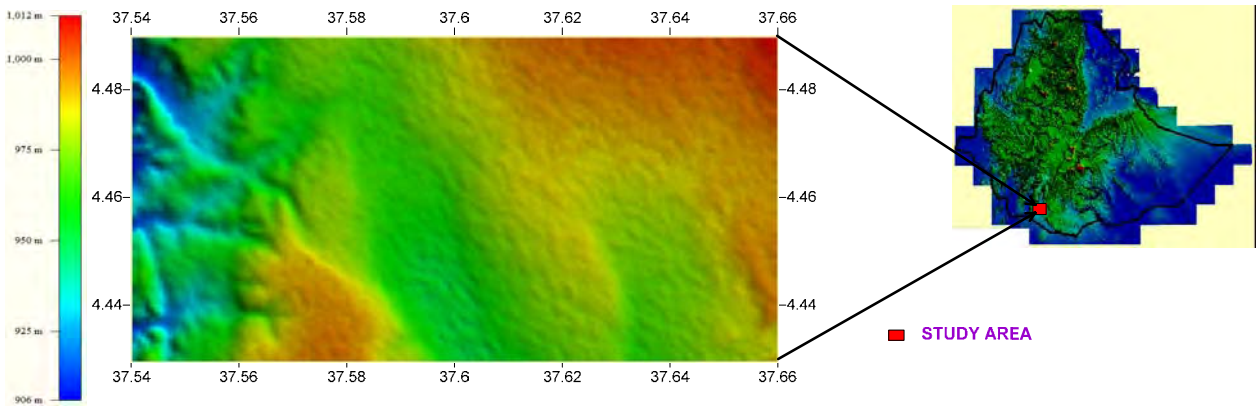

Figure 1.1Topographic map and Location of the study area using SRTM data

1.3 Climate and Vegetation

The climate of the study area is similar to the other region of Borena zone and it is characterized by arid to semi-arid climatic conditions with two rainy seasons. These are from March to May and September to November, but rarely with little rainfall from June to August whereas December and January are the hottest months .Although the mean monthly maximum and minimum temperature and annual precipitation data is not available for this study ,it is believed

that the amount of evaporation is greater than precipitation .The vegetation cover of the area is mostly continuous, dense and tall grass with thorny shrubs, wild seasonal, and scattered small trees. Burning of these bushes is commonly practiced by the pastoralist for the sake of free growing of grass for their livestock grazing. Land cultivation is relatively uncommon in the region, however small and limited farming is practiced to grow maize and sorghum at some location where settlement is existing .Drought and shortage of water extremely threatens the life of the people and livestock population. Drought is the major problem, which had been occurred at certain interval of time.

1.4 Geology of the study area

1.4.1Regional geology

Many researchers have done several studies at different time on geology of East Africa and particularly on southern Ethiopia and tried to explain the geology of the region. Three major rock groups namely Precambrian crystalline basement, Tertiary volcanic rocks and Quaternary volcanics and sediments constitute the regional geology of the project area (OWWDSE, 2008). The area is thus underlain by Proterozoic Metamorphic rocks and intrusives that are partly covered by Phanerozoic (pre-rift to post-rift) volcanic and superficial deposits. The Precambrian crystalline basement consists of older metamorphic complex, which include various gneisses, schists and granulites, intruded locally by suites of plutonic rocks. The gneisses and schists have been subjected mainly to middle amphibolite facies metamorphism. Some granulite facies rocks are exposed in structurally lower parts of the succession. The Precambrian basement rocks mainly occur in the eastern peripheries of the project area, stretching from north-eastern to south-eastern parts. Directly overlying the Precambrian Basement Complex are the Tertiary volcanic products. These consist of thick succession of flood basalt and overlying undifferentiated volcanic rocks of horizontally interbedded trachytes, trachy-basalt and rhyolite, intercalated with tuff and volcanic ash. These volcanic products are found in the western parts of the Borena zone, stretching from Marmaro to Taltalle. Most part of the project area is covered by horizontally layered sheets of extensive flood basalt of late Tertiary age, underlying low-lying plain areas between the Tertiary volcanic products from west and the Precambrian basement rocks from

east, extending in to Kenya towards south. Sporadically occurring throughout the area, recent volcanic activities took place during the Quaternary Period. These volcanic activities are characterized by volcanic cones and craters composed mainly of scoria and bedded tuff, with associated basalt flows that consist vesicular to scoraceous lavas with xenoliths of mantle nodules. Quaternary superficial deposits on the other hand occur in plain areas and stream channels (flood plains) mainly consisting of elluvial soils and alluvial deposits, with rarely occurring thin layers of calcrites and subordinate ferricrites. The main rifting event in southern Ethiopia took place within a period of some eight million years, 13-5 Ma ago; however, there is no obvious evidence of volcanism during this period (OWWDSE, 2008). Two different rift systems are known to occur in the project area: one is a N-S trending “Rirriba Rift” along which Rirriba River is aligned, and the other is a NW-SE trending “Mega Rift” that crosses areas in the vicinity of Mega Town (OWWDSE, 2008). According to the report, the Rirriba Rift System is characterized by low scarp normal faults that resulted in a half-graben. It is thought to be a direct southward continuation of the Main Ethiopian Rift System (MER). The Mega Rift System is characterized by high scarp (up to 1,000 m) normal faults, some of which are defined by aligned cinder and spatter cones and craters. These faults have produced narrow NW-SE horsts and grabens in the rift (OWWDSE, 2008). The Mega Rift is transverse to the Rirriba Rift System, and follows the Precambrian structural grain in the Yabelo area; it has a considerable southeast ward continuation beyond the project area.

In summary, the southern Ethiopia region is known mainly underlain by crystalline basement rocks of different deformational style and metamorphic grades and locally covered by younger volcanic rocks and classic sediments .Several intrusive bodies are also very common in the region .The out crops of the bed rocks are scarce at low lands and where the younger formations have widely covered. Most of the ridges and out crop patterns are seen mainly following the trends of the regional structures.

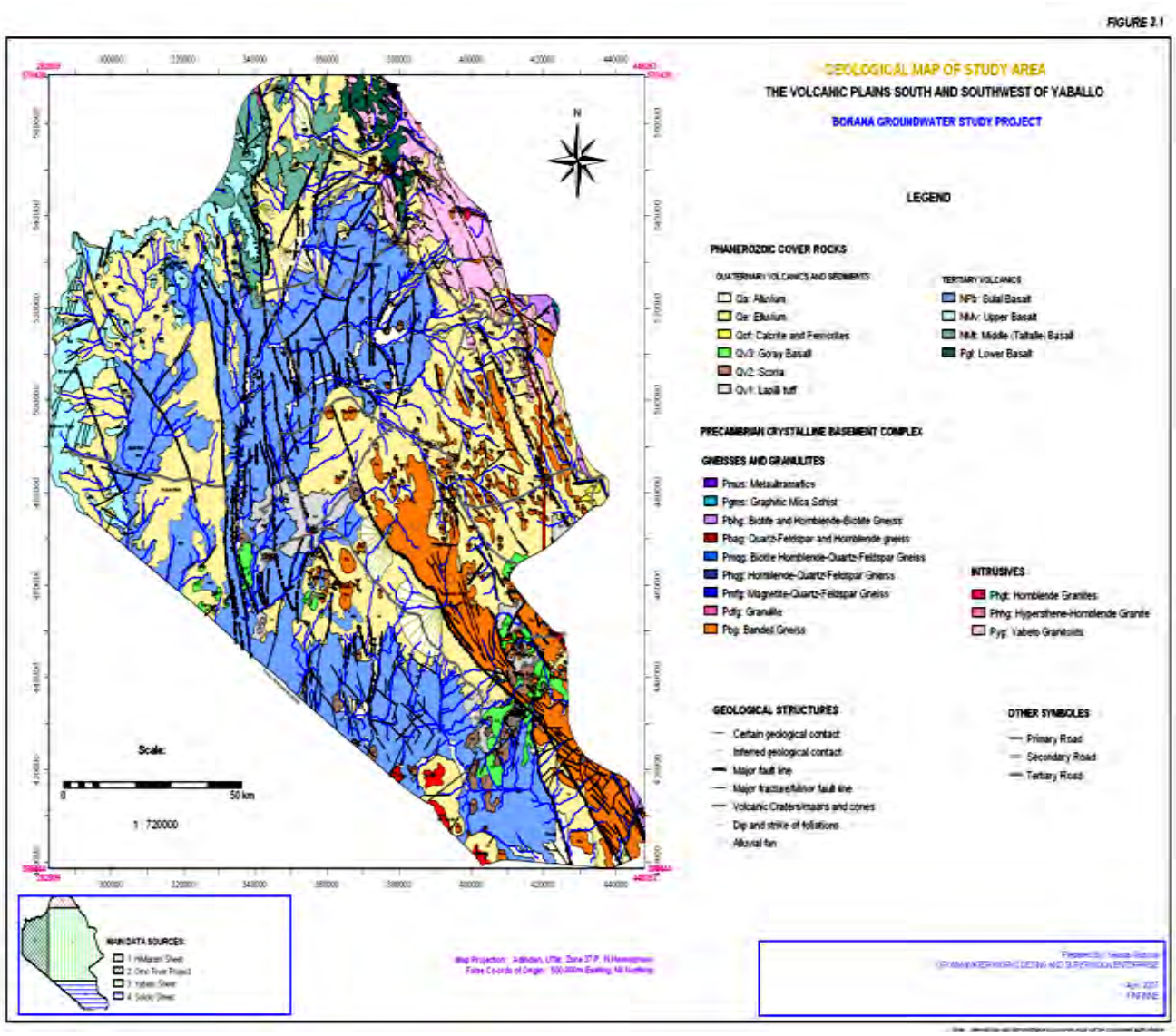

Figure 1.2 Regional Geological map (OWWDSE, 2008)

1.4.2 Local geology

Geologically, the area lies on volcanic terrain. The volcanic rocks are observed from the exposed out cropping rocks over the area and basaltic ridges around the area. The exposed basaltic formation over the area is highly vesicular and scoracious basalt. The observed volcanic rocks are also confirmed from the drilled well strata.

1.4.3 Hydrogeology

The water bearing capacity of volcanic rocks depends on mineralogy, texture, and rock structures. Circulation of ground water and storage capacity in volcanic rock depends on the type of porosity and permeability formed during and after rock formation (Mulugeta Chanie, 2010) The occurrence of groundwater in the basement and volcanic rocks is governed by the volume and behavior of faults, fissures, flow breccias, porous zones between successive lava beds, cracks and joints (Belete et al., 2000). The groundwater occurrences in the metamorphic rocks are in the fractured and weathered parts of the rock. In the case of volcanic rocks, the sizes of fractures are the predominant factors whereas for metamorphic rocks; the storage capacity is determined by the type of weathering products and the thickness of the consequent weathered layer. Metamorphic rocks are mostly impervious and serve as aquicludes and the only water bearing zones in many of them are the upper loose and weathered parts. Hence metamorphic rocks are characterized by secondary permeability which decreases with depth, the groundwater yield to wells decrease rapidly as depth increase

In general, the differently weathered and fractured basement and the contact between volcanic rock and the basement rock units are the potential aquifers for the drilled well in the area from the hydrogeologic point of view

1.4.4 Previous works

Various professionals had carried out several geological, geophysical, hydrogeological and engineering geology studies in different parts of southern Ethiopia in the past few decades. Detailed geological studies have been carried out for about half a century in different part of the region (Adola,Moyale,Hagara Mariam,Kenticha,Dawa,Digati and other localities) for purpose of gold and base metal exploration .Adola zone in particular has been extensively studied (Hussein, 1999). More detailed integrated geological studies were conducted, Kazmin (1971, 1972a). Later on, different authors with different scales conduct studies and present their result as; geology of Yabelo map sheet, NB 37-14 (Tesfaye Demissie, 2007); Borena groundwater project, detailed geological report (OWWDSE, 2008); hydrogeological, geophysical and engineering geological investigation of Yabelo map sheet, NB 37-14 (Belete et al., 2000).

1.5 Objective of the Study

1.5.1 General objective

The general objective of the survey is to get acquainted to the integrated geophysical methods and to reassess the general groundwater resources of the Wobok-Dilo area, through the combined usage of secondary data of gravity and electrical methods of prospecting as well as suggest preferred locations for the sinking of boreholes to extract the resource.

1.5.2 Specific objectives

To arrive at the goal set in the general objectives the following specific objective were set.

- To identify the subsurface electrical stratification and major subsurface geological units
- To determine the depth to groundwater table and locate potential drilling sites for extraction of groundwater

- To continuously map lateral variations and contacts between geologic units differing in mass and density resulting from subsurface weak zones which could serve as conduits for ground water movement
- Map the morphology of the basement rocks in the subsurface

1.6 Structure of the thesis

Chapter2, under the heading Theory and Methodology, reviews the theories and mathematical tools to describe both electrical and gravity methods of prospecting.

Chapter3, under the heading Data analysis and Processing, reviews the means of data analysis and how both the gravity and resistivity data have been processed, shows gravity data reliability by correlating the different gravity anomalies with height, and finally making the data ready for interpretation

Chapter 4, under the heading Result and Interpretation elaborate quantitative and qualitative interpretations which are model using and different anomalies maps that are produced by using different soft ware packages.

Chapter 5, under the heading Conclusion and Recommendation summarizes the conclusion of the thesis and recommend some potential site for extraction of ground water as well as additional future work to be carried out in the area.

CHAPTER 2

THEORY AND METHODOLOGY

2.1 Introduction

A jointed Gravity and Electrical Resistivity methods are used in this study .The gravity method is one of the potential field techniques that measures variation in Earth gravitation field at specific time and different location .The gravity method is used in ground water exploration to detect the structural trends controlling the ground water flows where as the resistivity method is used to delineate the possible aquifer zone and differentiating the subsurface layers .From electrical resistivity method one may get hydro geological information such as availability of ground water and water quality where as the gravity method is used to get information about the presence of structures such as faults, folds, aquifer bounding structures as well as to estimate depth to basement and their shape which are facts to assess the ground water potential zone in the given area.

2.2 Theory of Gravity Method

2.2.1 General

The gravity method is one of the potential field methods that measures variations in earth's gravitational field at specific location. In exploration geophysics, gravity surveying is conducted to investigate the subsurface geology based on variations in the earth's gravitational field caused by difference in density between rocks beneath the earth's surface. The gravitational attraction of a body of non homogenous density will vary from one measuring point to another due to

difference in the distribution of density in the body. These variations in gravitational attraction of the earth from point to point will provide valuable information about the subsurface geology. Gravity surviving uses gravity meters to measure these lateral variations in density. The final interpreted data will give a good structural trend of the subsurface rocks based on difference in density. Rock densities that give rise to gravity anomalies are among the least variable of all geophysical parameters (Robinson et al., 1988). The density of a rock depends on both its composition and porosity. Most common rock types have densities in the range between 1.6 and 3.2 g/cm3.

Gravity data in groundwater exploration should be collected in grid, scattered point or along profile .The most commonly used processed data are known as Bouguer anomalies commonly given in mgl or microgal. The interpretation of Bouguer gravity anomalies ranges just manually inspecting the grid or profile for variation in gravitational field to more complex method that involves separating the gravity anomaly due to object of interest from some sort of regional gravity field .To perform the later ,there are several manual and computer techniques including graphical ,smoothing and polynomial surface fitting .The interpretation of separated(residual) gravity anomalies commonly involves creating model of subsurface density variation to infer the geological set up underneath. These models can be determined using variety of methods ranging from analytical solution to simple geometry (e.g sphere) to complex three dimensional computer models. The theory and basic principle of the gravity method is described by different authors such as Telford et al., 1990; Dobrin, 1976; Parasnis,1962; Robinson et al., 1988; Reynolds,1997; Gibson and George, 2003 and Blakely, 1996 so that only short descriptions of this method is included in this thesis.

2.2.2 The Force of gravity

Gravity is the most conspicuous force present on surface of the earth .It is one of the fundamental forces on nature that controls all movement of mass on earth .Geophysical interpretations from gravity surveys are based on mutual attraction experienced by two masses as first given by Sir Isaac Newton.

Newton's law of universal gravitation state that the mutual attraction force between two point masses, M and m is proportional to the square of the distance R between them and directly proportional to the product of the two masses.

Considering that one of the masses is the Earth with mass M_E and the other mass m, we can write this statement mathematically as

$$\boldsymbol{F} = -\frac{\boldsymbol{GM_E}}{\boldsymbol{Re^2}}\boldsymbol{me_r} \qquad (2.1)$$

where, $\mathbf{e_r}$ is a unit vector extending outward from the centre of the Earth along the radius.

According to Newton's 2nd Law, an external force **F**, that sets a body of mass m, in to motion is

Force (F) = mass (m) X acceleration (a).

If the acceleration due to the attraction of the Earth is in a vertical direction then it is acceleration due to gravity (g),

$$\mathbf{F = mg} \qquad (\mathbf{2.2})$$

Combining equations (2.1) and (2.2) will give the magnitude of the gravitational force of attraction between M_e and m. Here it is assumed that the mass m is located on the surface of the Earth and the mass of the Earth (Me) is concentrated at its centre of mass. Then we can write

$$\mathbf{F = mg = G\frac{M_e m}{R_e^2}} \qquad (2.3)$$

and thus;

$$\mathbf{g = G\frac{M_e}{R_e^2}} \qquad (\mathbf{2.4})$$

where, g is the gravity force per unit mass or the gravity field intensity of the Earth.

Note, the negative sign is usually omitted since people usually speak of $|\boldsymbol{g}|$.

2.2.3 Units for Acceleration of Gravity

In the cgs system, the dimension of acceleration is cm/s^2, which is referred as gal, named after Galileo. The numerical value of g at the surface of the Earth is about 980 cm/s^2 (gals). In exploration work geophysicists are likely to be measuring differences in acceleration one-ten-millionth or less of the Earth's gravity field. This unit and its subdivisions commonly used by many geophysicists are defined as,

1 gal = 1 cm/s^2

1 gal = 1000 milligals (mgal)

1 gal = 10,000 gravity units (g.u.)

1 gal = 1,000,000 micro gals (μgal)

The SI units of acceleration are, 1 $m/s^2 = 10^2$ gal = 10^5 mgal = 10^6 g.u. = 10^8 μgal

2.2.4 Gravitational Potential

Gravity field can be represented by a scalar quantity called the gravitational potential. The gravitational potential, energy $U(R)$, is defined as the work done by a gravitational force to move a point mass from a very distant point (mathematically from infinity) by any path at all to a point distant, R, from the centre of gravity of M, It is given by:

$$\mathbf{U(r)} = \int_{\infty}^{\mathbf{R}} \mathbf{g}.\,\mathbf{dr} = -\mathbf{GM}\int_{\infty}^{\mathbf{R}} \frac{\mathbf{dr}}{\mathbf{r^2}} = \frac{\mathbf{GM}}{\mathbf{R}} \qquad (\mathbf{2.5})$$

Since the gravitational potential energy is a scalar quantity it is easier to determine the gravitational acceleration vector from the potential as:

$$\nabla \mathbf{U(r)} = {}^{\mathbf{F(r)}}/_{\mathbf{m}} = \mathbf{g(r)} \qquad (\mathbf{2.6})$$

As can be seen from the above equation g can be expressed in terms of a potential, U, therefore, gravity exploration is referred to as a potential – field technique.

Moreover, in gravity exploration we account only the vertical component of the gravity field g_z because it is the only direction in which g can be measured directly (Telford, et al 1980).

2.2.5 Three Dimensional (Newtonian) Potential

The potential at a point some distance **r** away from a three dimensional mass which has arbitrary shape can be calculated by first dividing the mass in to small element of mass dm and latter integrating it in order to get the total effect.

The potential of an element mass dm at a distance r from the centre of mass is:

$$\mathbf{dU = G\frac{dM}{r} = G\sigma\frac{dx\,dy\,dz}{r}} \qquad (\mathbf{2.7})$$

where,$\boldsymbol{\sigma}$ = density, and

$$r = (x^2+y^2+z^2)^{1/2}$$

Therefore, the potential of the total mass M is found as:

$$\mathbf{U(x,y,z) = G\sigma\int_x\int_y\int_z\frac{1}{r}\,dx\,dy\,dz} \qquad (\mathbf{2.8})$$

In cylindrical coordinates,

dV= r dr dφ dz, then u (r, φ, z) is:

$$\mathbf{U(r,\varphi,z) = G\sigma\int_r\int_\varphi\int_z drd\,\varphi dz} \qquad (\mathbf{2.9})$$

In spherical coordinates,

dxdydz = r^2 sinθ dr dθ $\mathbf{d\varphi}$,

Hence the potential in spherical coordinates will be,

$$\mathbf{U(r,\theta,\varphi) = G\sigma \int_r \int_{\varphi} \int_{\theta} r2\ sin\theta dr d\theta d\varphi} \qquad (\mathbf{2.10})$$

Since the gravity field can be derived from the scalar gravitational potential then, the acceleration in the vertical (Z) direction which is the only component of g that can be measured directly will be,

$$\mathbf{g_z = \frac{\partial U}{\partial Z}} \qquad (\mathbf{2.11})$$

In Cartesian coordinate system,

$$\mathbf{g_z = -G\sigma \int_x \int_y \int_z \frac{Z}{r^3}\ dx\ dy\ dz} \qquad (\mathbf{2.12})$$

In Cylindrical coordinate system,

$$\mathbf{g_z = -G\sigma \int_r \int_{\varphi} \int_z \frac{Z}{r^2}\ dr\ d\varphi\ dz} \qquad (\mathbf{2.13})$$

In Spherical coordinate system,

$$\mathbf{g_z = -G\sigma \int_r \int_{\varphi} \int_{\theta} \sin\theta\ cos\theta\ dr\ d\varphi\ d\theta} \qquad (\mathbf{2.14})$$

Note: In the above equations (2.12, 2.13 and 2.14) the density assumed to be constant throughout the volume.

2.2.6 Two Dimensional (Logarithmic) Potential

Consider a two dimensional body which has arbitrary shape. If the mass is very long in the Y – direction and has uniform cross section in the XZ plane, then the gravity attraction derives from a logarithmic potential.

The logarithmic potential expression becomes:

$$\mathbf{U(x,z) = 2G\sigma \int_X \int_Z \log \frac{1}{r}\, dx\, dz} \qquad (\mathbf{2.15})$$

Therefore, the gravity effect of the two dimensional body will be:

$$\mathbf{g_z = \frac{\partial U}{\partial Z} = -2G\sigma \int_x \int_z \frac{z}{r^2}\, dx\, dz} \qquad (\mathbf{2.16})$$

where, $\mathbf{r = (x^2 + z^2)^{1/2}}$ This equation is used for calculating the gravity effects of bodies of uniform density and regular shape such as, sphere, cylinder, horizontal slab etc.

2.2.7 Geometry of the Gravity Field

2.2.7.1 Gravity of a Rotating Sphere

Consider the Earth as a rotating spherical body which is rotating with angular velocity ω. If a small mass, m, is moving with a velocity V on the surface of the earth, then the net acceleration acting on the mass, m, is given by:

$$\mathbf{g = g_m + g_\omega + g_c + T} \qquad (\mathbf{2.17})$$

where,

$\mathbf{g_m = G\,(Me/R_e^2)}$ is the attraction force per unit mass acting on m due to Earth's mass.

$\mathbf{g_\omega = \omega\,(\omega \times R_e)}$, is the centrifugal force per unit mass due to Earth s rotation with ω.

$\mathbf{g_C = 2(\omega \times V),}$ is the Coriolis acceleration resulting from the Coriolis force. If the mass, m, is at rest v becomes zero, then $g_C = 0$.

T is the tidal force, which is caused by the heavenly bodies. It is difficult to express the tidal force by a simple formula because the heavenly bodies are always in motion with respect to the mass, m.

The effect of g_C on g is usually considered negligible. Therefore, gravity refers to the combined effect of both Earths mass gravitational acceleration centrifugal acceleration and tidal force.

The centrifugal acceleration of the earth is acting perpendicular to the axis of rotation of the earth. Our interest is to get the radial component of, g_ω which is acting in the opposite direction of the mass gravitational acceleration.

Therefore, the vertical component of the acceleration of gravity g can be found as:

$$\mathbf{g = g_m + g_\omega + T = G\frac{m}{r^2} - \omega^2 r \cos^2 \varphi - T} \qquad (\mathbf{2.18})$$

where **φ** is the latitude on which the mass m is found with respect to the centre of the earth. The above equation indicates that the variation of g on the earth's surface depends on **φ**.

1 m/s^2 = 10^2 gal = 10^5 mgal = 10^6 g.u. = 10^8 μgal

2.2.8 The Earth's Figure and Gravity

The ellipsoidal shape of the Earth with the widest portion of the ellipsoid aligning with the equator was first proposed by Isaac Newton in 1687.

The shape of the Earth and gravity has a close relationship. The shape of the Earth is distorted from a spherical shape due to its rotation. The best mathematical approximation to the figure of the earth is an oblate ellipsoid .This can be referred as the International Reference Ellipsoid.

The dimension of the reference ellipsoid has been refined continually as more exact data have become available. In 1980 at the International Union of Geodesy and Geophysics (IUGG) geodesists and geophysicists agreed to take ellipsoid that has equatorial radius (a), 6378.136 km and polar radius (b), 6356.751 km, as a reference Ellipsoid GRS80, where as the radius of the equivalent sphere is 6371.000 km.

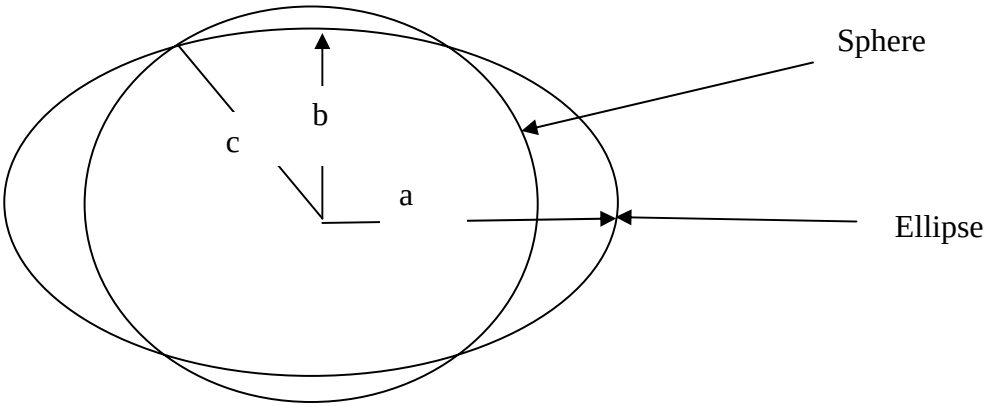

Figure 2.1 Comparison of the dimensions of the international reference ellipsoid of 1980,

with a sphere of equal volume.

The polar flattening (f) is defined as:

$$\mathbf{f} = \frac{\mathbf{a-b}}{\mathbf{a}} \qquad (\mathbf{2.19})$$

The surface of the ellipsoid is to be a level surface in the normal gravity field (Torge, 1989). The earth's gravity potential (W) on the surface of the earth consists of the mass gravitational potential (U_m) and the centrifugal potential (V_Φ).

The centrifugal potential arises from the radial component of the centrifugal acceleration.

Therefore,

$$\mathbf{W = U_m + V_\varphi} \qquad (\mathbf{2.20})$$

$$\boldsymbol{W(X,Y,Z) = G \iiint \sigma \frac{dy}{z} + \frac{1}{2}\omega^2 (X^2 + Y^2)} \qquad (\mathbf{2.21})$$

The relationship between gravity and gravity potential is:

$$\mathbf{g = grad\ W} \qquad (\mathbf{2.22})$$

2.2.9 Equipotential Surfaces and Plumb lines

The gravity field can be geometrically described by surfaces of constant gravity potential (equipotential or level surfaces)

$$W(r) = \text{const.}$$

and by plumb lines. The relationship between changes in potential and changes in position follows from the relation, **g = grad W**.

$$\mathbf{dW = g.dr = gdrcos(g, dr)} \qquad (\mathbf{2.23})$$

If a test mass is moved along a level surface, we have **dW = 0**. As a result no work is performed; the level surfaces are equilibrium surfaces.

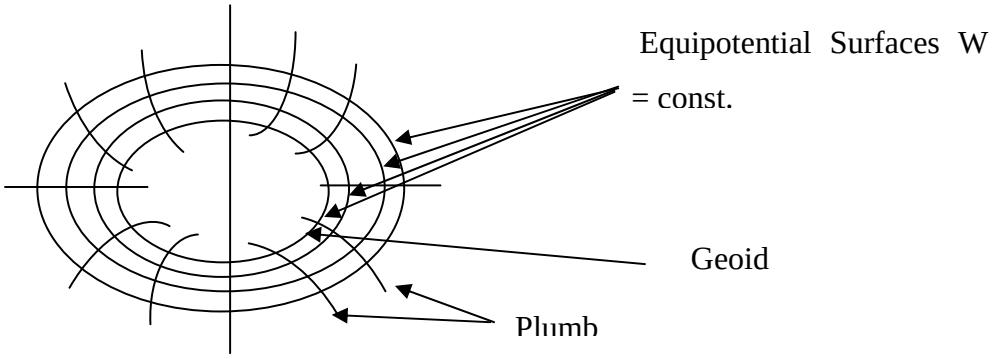

Figure2.2 Equipotential surfaces and plumb lines near the Earth's Surface.

The plumb lines intersect the level surfaces perpendicularly.

Differentiating the gravity potential **W = W(x, y, z),** we will get,

$$\mathbf{dW = \frac{\partial W}{\partial X} dx + \frac{\partial W}{\partial Y} dy + \frac{\partial W}{\partial Z} dz} \qquad (\mathbf{2.24})$$

If the vector ds is taken along the equipotential surface W = Wo, then the potential remains constant and dW = 0, i.e.

$$\mathbf{dW = gradW.ds = g.ds, then\ g.ds = 0} \qquad (\mathbf{2.25})$$

Since gravity varies due to factors such as variation in mass distribution, the level surfaces are not parallel. The level surface which approximates mean sea level is denoted as geoid. It serves as a reference surface for defining height systems (Torge, 1989).

Geoid is defined as an equipotential surface corresponding with mean sea level surface. The mean sea level is considered because the oceans are subject to tides and currents. For practical work, measurements of gravity is carried on the physical equipotential surface i.e. geoid or on its best approximation, the ellipsoid.

The theoretical value of gravity γ_Φ on the rotating ellipsoid can be computed by differentiating the gravity potential W and thus,

$$\mathbf{g_\varphi = gradW} \qquad (\mathbf{2.26})$$

If one is considering a rotating ellipsoid, W will be the potential due to the attracting mass and rotation. Making the necessary mathematical treatment we will arrive at the variation of the theoretical gravity value $\boldsymbol{\gamma_\Phi}$ that is normal to the ellipsoid surface. This value is given as:

$$\boldsymbol{\gamma_\varphi = \gamma_e\,(1 + \beta sin^2\Phi - \beta_1 sin^2 2\Phi)} \qquad (\mathbf{2.27})$$

where, γ_e is the value of gravity at the equator $\Phi = 0$, $\boldsymbol{\beta}$ = gravity flattening and $\boldsymbol{\beta_1}$ is computed from the flattening f and the ratio of equatorial centrifugal acceleration and equatorial gravity (m).

The mathematical formula used to predict the components of the gravitational acceleration produced by the earth's shape and rotation is called the Geodetic Reference Formula. The predicted gravity is called the normal gravity.

The formula for calculating the normal gravity γ_Φ at any latitude, Φ, on a rotating ellipsoid was revised in 1967 by the International union of Geodesy and Geophysics (IUGG). Incorporating the parameters;

Re = 6,378,160 meters

Rp = 6,356,774.5 meters

f = 1/298.247

ω = 7.2921151467 x 10^{-5} radian/second

γ_e = 978.031846 gals

Table 2.1 Normal Gravity Formulas (Torge, 1989).

Name	γ_e	β	β_1	f
HELMERT (1901)	9.78003	0.005302	0.000 007	1:298.3
U.S. Coast and Geodetic Survey (BOWIE 1917)	9.78039	0.005294	0.000007	1:297.4
Intern. Gravity Formula (CASSINIS 1930)	9.78049	0.0052884	0.0000059	1:297.0
Geoid. Ref. System 1967 (INT. ASS. GEOD. 1971	9.780318 (incl. atmosph. mass)	0.0053024	0.0000059	1:298.247
Geoid. Ref. System 1980 (MORITZ 1984)	9.780327 (incl.atmosph. mass)	0.0053024	0.0000058	1:298.257

In the normal gravity formula, $\boldsymbol{\gamma_\Phi = \gamma_e (1 + C_1 \sin^2\Phi + C_2 \sin^4\Phi),}$ Where, the constants C_1 and C_2 depend on the flattening f and the rate of rotation ω. We will get;

$$\boldsymbol{\gamma_\Phi = 978.031846(1 + 0.005278895 \sin^2\Phi + 0.000023462 \sin^4\Phi)} \qquad (\mathbf{2.28})$$

The above equation is called the 1967 Geodetic Reference System (GRS67) formula (Robinson, 1988). The normal gravity formula **(γ_e)** that was used as a reference for our gravity data reduction is the Geodetic Reference System, GRS80 formula by (Moritz, 1984).

$$= \boldsymbol{\gamma_e} \frac{\mathbf{1} + \boldsymbol{\kappa sin^2 \varphi}}{(\mathbf{1} - \boldsymbol{e^2 sin^2 \varphi})^{\mathbf{2}}} \qquad (\mathbf{2.29})$$

where, $\gamma_e = 9.7803267715\ ms^{-2}$

$\kappa = b\ \gamma_p / a\ \gamma_e - 1 = 0.001\ 931\ 851\ 353$

$e^2 = a^2 - b^2 / a^2 = 0.006\ 694\ 380\ 0229$

2.2.10 Gravity Reference Systems

Since spring gravimeters measures the relative gravity values between observation sites, it is important to find the absolute gravity values at the observation point. In order to determine the absolute gravity value at the observation point at least one gravity base station is needed, where its absolute gravity value is known.

The absolute gravity value at each station can be determined by tying it with the global reference system, the International Gravity Standardization Net, 1971(I.G.S.N.71) (Morelli et al, 1974).

Hence, the absolute gravity (g) value at the observation site can be found by;

$$\mathbf{g} = \mathbf{g_r} + \Delta\mathbf{g} \qquad (\mathbf{2.30})$$

where, g_r is the absolute gravity value at the base station; Δg, the gravity difference between the base station and the observation site after corrected for, tide and drift. (Robinson et al, 1988).

2.2.11 Gravity Reductions

In gravity surveys, field work is carried on land by taking gravity readings on a profile, at grid stations or scattered points covering an area of interest with station interval that takes into

consideration the frequencies of interest to be observed. In all gravity surveys the vertical component of g, g_z, is measured. A gravity survey shows variation in the g_z reading which is caused by, instrumental drift, earth tides, local topography or terrain, and variation in subsurface density. Therefore, in order to see the desired anomaly which is caused by variations of subsurface density, it is important to correct the other factors that affect the value of g_z. In general all gravity values are reduced to a datum plane, but this plane need not necessarily be the sea-level surface (Dobrin, 1988). Those factors which affect the gravimeter readings are classified as temporal and spatial variations.

2.2.11.1 Temporal Variations

The temporal variation includes the time varying factors: namely instrumental drift, tare and tidal effects, and pressure effect.

2.2.11.2 Drift and Tare Correction

Instrumental drift is the time dependent mechanical changes within the gravimeter even though the gravimeter is handled with care. These variations in the gravimeter spring properties with time can be due to stretching of the spring, associated with temperature and/or pressure changes.

Because of instrumental drift repeated observations at one location yield different values for the gravitational acceleration. The gravimeter is usually read more times a day for several days. To correct the change in gravimeter reading that is caused by instrumental drift or tare, the usual practice is to reoccupy one or more stations periodically during a gravity survey. Repeated gravity readings at one station will give a series of different gravity values, which is useful to produce a drift curve for the instrument. In order to determine drift effect properly, we should make gravimeter readings at one to three hour intervals (Robinson, 1988).

Another unwanted and more serious problem that needs a special treatment is the tare effect. A tare occurred due to an abrupt change in the gravimeter reading. Gravity variation of several tenths of mgal or more may occur due to tare effect (Robinson, 1988). Repeated reading at one or more stations and a careful analysis of the drift before and after the tare effect is needed to remove its effect from measurements.

In high precision surveys measurements will be taken repeatedly in more than one point and adjustment of measurements will be carried out using computer programs aided with visual control of tare effects (Becker, 1984).

2.2.11.3 Tide Correction

Tides are caused by variations in gravity observations resulting from the attraction of the celestial bodies (moon and sun). The Earth's body experiences an elastic deformation due to the tidal forces (Earth body tides) (Torge, 1989). The resulting bulges in the surface have diurnal periodicity which is predictable at any point on the surface of the Earth. The tidal variations can be on the range of 0.2 to 0.3 mgal (Dobrin, 1988). So to use the full sensitivity of the gravimeter these variations must be removed.

In some small scale surveys it may be reasonable to assume that the tidal variations are linear with time during the intervals between the times that a base or reference station is reoccupied. In this case the tidal variations are included and treated in the same manner as the slow drift in gravimeter readings caused by inherent strain in the sensing element.

The tidal variation of gravity which is obtained by a gravimeter survey can be corrected based on the masses of the sun and moon and their positions relative to an observation site. This can be computed by the formula:

$$\delta g_T = \frac{3}{2}\,\sigma G R \left[\frac{M_m}{r_m^3}\left(\cos 2\theta_m + \frac{1}{3}\right) + \frac{M_s}{r_s^3}\left(\cos 2\theta_s + \frac{1}{3}\right)\right] \qquad (2.31)$$

where, R, is the earth's radius, M_m and M_s are the lunar and solar masses and their distances from the earth s centre are r_m and r_s. The value $\sigma = 1.16$ accounts for the way that the Earth itself is

stretched elastically by the tidal force. Angles θ_m and θ_s, between a line from the Earth's centre to the observation site and lines from the earth's centre to the moon and sun change with time. These formulas are long and complicated; a computer program is ordinarily used to make the calculations (Robinson, 1988).

A more accurate way of removing the tidal effect is through the usage of tidal models such as Dodson, Cartwright etc (Torge, 1989).

2.2.11.4 Pressure Correction

Fluctuation of the atmospheric pressure changes the buoyancy of the gravimeter mass. For a known distribution of the atmospheric pressure, the gravitational effect can be computed by evaluating the law of gravitation. In order to correct the variation in gravity reading caused by atmospheric pressure, the atmospheric pressure must be measured by the barometer.

After a certain computation, the direct gravitational effect of the atmospheric pressure will be;

$$\boldsymbol{\delta g_{atm} = -2\Pi \frac{G}{g} \delta p = -4.3 \delta p \ nms^{-2}} \qquad (\mathbf{2.32})$$

where $\boldsymbol{\delta p}$ is given by in hpa (Torge, 1989).

With increasing size of the effective of air masses, the deformation effect increases, this acts in opposite direction. Model computations have resulted in

$$\boldsymbol{\delta g_{atm} = -3.0 \delta p \ nms^{-2}} \qquad (\mathbf{2.33})$$

For the time-average of non-tidal atmospheric effects on the gravity value, with $\boldsymbol{\delta p}$ in hPa .

2.2.11.5 Spatial Based Variations

These are changes in the observed gravitational acceleration that are space dependent. Just like the geologic effects, these change the gravitational acceleration from place to place, but these are not related to the subsurface geology.

2.2.11.6 Freeair Correction (δgFA)

In this case, the topographical masses above mean sea level (datum) surface up to the observation point is ignored. The observation point is thought as if it is suspended in the air and, hence the name freeair. In changing elevation, g_z, changes because of the change in distance from the centre of mass of the earth up to the gravity observation point. Therefore, it is necessary to correct for changes in elevation between stations. As a result all field readings are reduced to a datum surface.

From Newton's law we have that, $\mathbf{g_z = G\frac{M_e}{R_e^2}}$ differentiating this equation with respect to R_e we will get the value of the free air correction as:

$$\mathbf{\delta g_{FA} = \frac{dg_{FA}}{dR_e} = -\frac{-2M_e}{R_e^3} \approx -\frac{2g}{R_{eq}} \approx -0.3086 mgal/m} \qquad (2.34)$$

where, $\mathbf{\delta g_{FA}}$ is the free air correction and $\mathbf{R_{eq}}$ is the equivalent radius.

As the negative sign implies, the freeair correction is added to the field reading when the station is above the datum plane and subtracted when below it. In order to apply freeair correction the station height must be precisely known. **.**

Note: If the gravity measurement accuracy is about 0.01 mgal, which is the sensitivity of the most of the present day gravimeters, then we must know our elevation to 2 inches (5.08cm) (Telford et al, 1990).

2.2.11.7 Bouguer Correction (δgB)

The Bouguer correction is a correction to account for the excess mass underlying observation points located at elevations higher than the elevation datum (sea level or the geoid). Conversely, it accounts for a mass deficiency at observation points located below the elevation datum. The two assumptions that are useful in deriving the Bouguer correction are, the slab is made of uniform density and it has infinite horizontal extent. As one changes elevation there are changes in g caused by the added (or subtracted) layer of material that has been included. Thus in moving up from a valley to a plateau the gravity decreases due to the increasing distance from the centre of mass but it also increased by the attraction of the slab of rock whose thickness is the change in elevation.

The gravitational attraction of an infinite slab of thickness **Δz** and density **σ** is:

$$\boldsymbol{\delta g_B = 2\pi G \sigma \Delta z = 0.04193 \sigma \Delta z} \qquad (\mathbf{2.35})$$

where **σ** is in gm cm^{-3}, Δz is in meters and $\boldsymbol{\delta g_B}$ is the Bouguer correction. (Robinson et al, 1988). If we assume that the slab has density of 2.67 gm cm^{-3}, the Bouguer correction will be δg_B = 0.1118 mgal /m.

The effect of this intervening slab is called the Bouguer effect and the correction is called simple Bouguer correction. It is the opposite sign to the free air correction. This effect may be difficult to calculate because one does not know the density. Furthermore, if the elevation change is confined to a small region, like going up a hill, then the infinite slab is an inappropriate description of the intervening mass. Under this circumstance the actual topography must be considered and another effect, the terrain effect, is included. Conventional practice is to apply the Bouguer correction first and, the terrain correction.

2.2.11.8 Terrain Correction (δgT)

The Terrain correction accounts for variations in the observed gravitational acceleration caused by variations in topography near each observation point. With considerable topographic relief the infinite Bouguer slab is not a good model for the intervening mass between the reference elevation and the point of observation. The actual gravitational effects must be calculated numerically for the masses above and below the slab surface.

In Figure (2.3), M_1 is a mass excess adjacent to the observation point which reduces the value of g_z. M_2 is a mass deficit adjacent to the observation point which also reduces the value of g_z. Similar to the Bouguer reduction it is necessary to determine the appropriate density values of the surrounding lithologic units to carry out terrain reduction. The terrain corrections are difficult to do in very rugged terrain because the nearest features have the biggest effect. Choosing the density is also a problem but an iterative process is used until the corrected data shows no correlation with the topography.

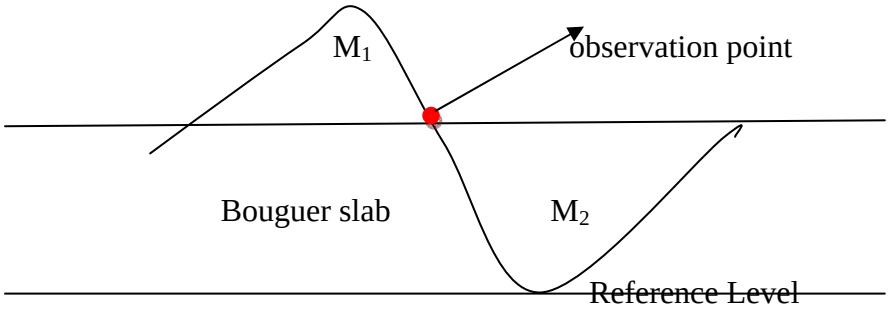

Figure 2.3 Topographic effects of the valley (M_2) and the mountain (M_1) on the gravity observation point.

When the terrain in the vicinity of the observation point is rugged, the whole area is represented by concentric circles and radial lines, making sectors whose areas increase with distance from the centre. The gravity effect of a single sector can be calculated from the formula:

$$\boldsymbol{\delta gt\,(r,\theta) = \sigma G\theta \left\{(r_o - r_i) + \frac{\left(r_i^2 + z^2\right)}{2} - \frac{(r_o^2 + z^2)}{2}\right\}} \qquad (2.36)$$

where; θ = sector angle (radians), z = le_s – e_al, e_s = station elevation, e_a = average elevation in sector, r_O and r_i = outer and inner sector radii respectively (Telford, et a, 1990).

The terrain correction is the sum of all the sectors. Therefore, if we have n number of sectors, the total terrain correction will be:

$$\delta g_T = n\, \delta gt\,(r, \theta) \qquad (2.37)$$

Nowadays, it is customary to model the topography of the survey area and its surrounding using parallelepipeds (Nagi, 1966; Banerjee and das Gupta, 1977) and compute the effect of each parallelepiped at measurement points to carry out terrain reduction.

Because of the assumptions made during the Bouguer Slab correction, the terrain correction is positive regardless of whether the local topography consists of a mountain or a valley region. As a result the terrain correction is always added to the station reading.

2.2.12 Gravity Anomaly

The word anomaly implies deviation from the expected values caused by known effect. Gravity anomalies (Freeair and Bouguer) are geophysical tools up on which effects of geology on the earth's gravity field can be detected.

If g_{obs} is the measured gravity value at station elevation h above the reference ellipsoid, it should be reduced to reference ellipsoid to compare it with g_Φ, the theoretical value on reference ellipsoid of the same latitude Φ. Therefore the gravity anomaly at a station is defined by,

$$\Delta g = g_{obs} - \gamma_\Phi \qquad (2.38)$$

where; **Δg is** the gravity anomaly; g_{obs} is the measured gravity value of a station reduced to the ellipsoid surface, after the temporal and spatial corrections have been applied; γ_Φ, the theoretical gravity of the station at latitude, **Φ**.

In order to get the desired anomaly that is caused by geologic structure, we have to correct the measured gravity value, for the corrections that we have mentioned before. Therefore:

The Free - air anomaly (Δg_{FA})

$$\Delta \mathbf{g_{FA}} = \mathbf{g_{obs}} + \mathbf{0.3086h} - \boldsymbol{\gamma}_{\mathbf{\Phi(1980)}}\,(\mathbf{mgal}) \qquad (\mathbf{2.39})$$

where, h is the elevation at which the gravity station is above the datum chosen for the survey.

The Bouguer Anomaly (Δg_B)

$$\Delta \mathbf{g_B} = \mathbf{g_{obs}} + \mathbf{0.3086h} - \mathbf{0.04193\,\sigma\,\Delta z} - \boldsymbol{\gamma}_{\mathbf{\Phi(1980)}}\,(\mathbf{mgal}) \qquad (\mathbf{2.40})$$

The complete Bouguer Anomaly (Δg_T)

$$\Delta \mathbf{g_T} = \mathbf{g_{obs}} + \mathbf{0.3086h} - \mathbf{0.04193\,\sigma\,h} + \boldsymbol{\delta}\mathbf{g_T} - \boldsymbol{\gamma}_{\mathbf{\Phi(1980)}}(\mathbf{mgal}) \qquad (\mathbf{2.41})$$

Note: Considering that the above corrections have accurately accounted for the variations in gravitational acceleration due to known facts that are not related with the goal of the thesis can now be assumed to be caused by geologic structures.

2.2.13 Bouguer Anomaly Accuracy

The accuracy of the Bouguer anomaly is determined by the amount of errors which were propagated from the measured value to the Bouguer anomaly. Error on Bouguer anomalies arises from the precision in determining latitude, elevation, reduction density, the observed gravity and the accuracy of the instrument used in the survey.

Since the Bouguer anomaly is a function of $\Delta g = \Delta g\ (g, h, \Phi, \rho)$, then the partial differentiation of the Bouguer anomaly formula (equation) with respect to the above mentioned parameters will give as the propagation of the error during the different data reduction**.**

$$\boldsymbol{d}\Delta\mathbf{g} = \mathbf{R}_{\Delta\mathbf{g}} = \frac{\partial \Delta \mathbf{g}}{\partial \mathbf{g}}\,\mathbf{dg} + \frac{\partial \Delta \mathbf{g}}{\partial \mathbf{h}}\mathbf{dh} + \frac{\partial \Delta \mathbf{g}}{\partial \boldsymbol{\rho}}\mathbf{d}\boldsymbol{\rho} + \frac{\partial \Delta \mathbf{g}}{\partial \boldsymbol{\varphi}}\mathbf{d}\boldsymbol{\varphi} \qquad (\mathbf{2.42})$$

$$\mathbf{R_{\Delta g}} = \frac{\partial \Delta \mathbf{g}}{\partial \mathbf{g}} \mathbf{r_g} + \frac{\partial \Delta \mathbf{g}}{\partial \mathbf{h}} \mathbf{r_h} + \frac{\partial \Delta \mathbf{g}}{\partial \boldsymbol{\rho}} \mathbf{r_\rho} + \frac{\partial \Delta \mathbf{g}}{\partial \boldsymbol{\varphi}} \mathbf{r_\varphi} \qquad (\mathbf{2.43})$$

where, r_g = gravity observation error, r_h = elevation error r_ρ = density error and r_Φ = latitude error, are the standard errors.

The variance of the standard error $\mathbf{R_{\Delta g}}$ can be computed from the law of propagation of errors for uncorrelated observations as;

$$\boldsymbol{R^2_{\Delta g}} = \boldsymbol{r_g^2} + \left(\frac{\partial \Delta \mathbf{g}}{\partial \mathbf{h}}\right)^2 \mathbf{r_h^2} + \left(\frac{\partial \Delta \mathbf{g}}{\partial \boldsymbol{\rho}}\right)^2 \mathbf{r_\rho^2} + \left(\frac{\partial \Delta \mathbf{g}}{\partial \boldsymbol{\varphi}}\right)^2 \mathbf{r_\varphi^2} \qquad (\mathbf{2.44})$$

This being the standard error, the overall mean square error $\boldsymbol{\sigma^2}_{\Delta \mathbf{g}}$ of the Bouguer anomaly becomes;

$$\boldsymbol{\sigma^2_{\Delta g}} = \mathbf{R^2_{\Delta g}} + \mathbf{S^2_{\Delta g}} \qquad (\mathbf{2.45})$$

where, $\mathbf{S^2}_{\Delta \mathbf{g}}$ is the systematic or bias error of the gravity anomalies.

2.3 Theory of Electrical Resistivity Method

2.3.1 General

Electrical resistivity methods have been used in a number of groundwater exploration surveys when the resistivity of the rocks is needed to be inferred. The resistivity of shallow subsurface of the Earth which yields much of our groundwater resources depends on the clay content, formation porosity, amount of water in the rock and the salinity of the water in the rocks. The electrical conductivity of these rocks will increase when they are saturated well with water compared to unsaturated and dry rocks. The resistivity of the saturated rocks in the upper part of the earth's crust, decreases with increasing their porosity and the degree of salinity of the saturated fluids. In contrary to the above, the presence of clay and conductive minerals can also reduce the rocks which can be resolved by using other geophysical techniques, geological or well information. In resistivity surveying especially in vertical electrical sounding (VES), conduction in rocks is mainly due to pore fluids acting as electrolytes. Water in its pure form is poor

conductor but most water contains dissolved salts which facilitate current flow. The resistivity of geological materials exhibits one of the largest ranges of all physical properties from 1.6 x 10-8 Ω m for native silver to 1016 Ω m for pure sulphur (Reynolds, 1997). The theory and basic principle of electrical resistivity method was described by different authors such as Telford et al, 1990, Dobrin and Savit, 1976; Parasnis, 1962; Robinson and Caruh, 1988; Reynolds, 1997; Gibson, and George, 2003 so that only short descriptions of this method is included in this thesis.

2.3.2 Basic principle of Electrical (DC) Resistivity Method

The electrical conductivity of rocks can be studied by measuring the electrical potential distribution produced at the earth's surface due to an electric current which is injected in to the ground through electrodes for the cause of DC current. The types of currents introduced in to the ground are direct, commutated or low frequency alternative currents and the potential difference are measured using non-polarized electrodes. The direct current sources are used to inject current in to the ground using two current electrodes to measure the generated electric field as a potential difference using other two potential electrodes .If we consider the media that the current entered as a homogeneous isotropic ground, the flow of current in the medium is based on the principle of conservation of charge and is expressed by the relation

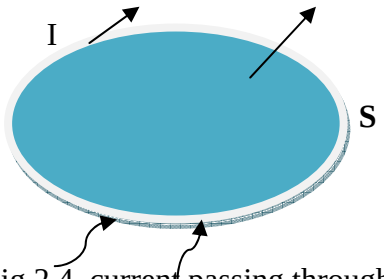

Fig 2.4 current passing through surface s.

$$(I_c)_s = \frac{-dQ}{dt} \qquad (2.46)$$

where I_c is the current flowing out of the closed surface 'S' and 'Q' is the charge enclosed by 'S'. The current I_c and total charge Q can be expressed in terms of the current density **J** (the current

Ic divided by the area over which the current is distributed) and the charge density **q** which is the total charge Q divided by the volume V as

$$(\boldsymbol{I_C})\boldsymbol{S} = \oint \boldsymbol{J}.\boldsymbol{ds} \qquad \boldsymbol{and} \quad \boldsymbol{Q} = \int_v \boldsymbol{qdv} \tag{2.47}$$

where 'v' is the volume bounded by the surface, substituting the above equation in two equation (2.46) and further more applying the divergence theorem we reach at

$$\int_v (\boldsymbol{\nabla}.\boldsymbol{J})\boldsymbol{dv} = -\int_v (\frac{\boldsymbol{\partial q}}{\boldsymbol{\partial t}})\boldsymbol{dv} \qquad \boldsymbol{or} \quad \int_v (\boldsymbol{\nabla}.\boldsymbol{J} + \frac{\boldsymbol{\partial q}}{\boldsymbol{\partial t}})\boldsymbol{dv} = \boldsymbol{0} \tag{2.48}$$

Equation (2.42) is valid for any volume so that we can write it as

$$\boldsymbol{\nabla}.\boldsymbol{J} + \frac{\boldsymbol{\partial q}}{\boldsymbol{\partial t}} = \boldsymbol{0} \tag{2.49}$$

Equation (2.49) is called the law of conservation of charge in differential form and also known as continuity equation

For direct current, $\frac{\partial q}{\partial t} = o$ so equ (2.49) reduce to the form

$$\nabla.J = 0 \tag{2.50}$$

The electric field **E** is conservative field, it can be expressed as gradient of the scalar potential function v as

$$\boldsymbol{E} = -\boldsymbol{\nabla v} \tag{2.51}$$

where 'V' is measured in volts. From ohm's law; R=V/I, where V and I are the potential difference across with resistance **R**(Ω) and current passing through it respectively .This expression can be written alternatively in terms of electric field strength **E**(volt/m) and current density **J**(amp/m^2) as

$$\rho = \frac{\boldsymbol{E}}{\boldsymbol{J}}(\Omega \text{ m}) \tag{2.52}$$

by taking only their magnitudes, the relation between the current density (J)and electric field intensity (E) can be given as

$$\boldsymbol{J = \frac{1}{\rho} E = -\frac{1}{\rho} \nabla v} \qquad (\mathbf{2.53})$$

where ρ is scalar function of the point of observation and it is in the same direction as the **E** for isotropic medium .From equ (2.50) and (2.53) we have

$$\boldsymbol{\nabla \frac{1}{\rho} . \nabla v + \frac{1}{\rho} \nabla . \nabla v} = 0 \qquad (2.54)$$

This equation is called the fundamental equation of electrical prospecting with direct current.

For homogenous medium, **ρ** is independent of the coordinate axes and equation (2.54) is simplified as

$$\nabla . \nabla V = 0 \quad \text{or } \nabla^2 V = 0 \qquad (2.55)$$

This is called the Laplace equation.

Therefore, the electrical potential distribution for direct current flow in a homogeneous isotopic medium satisfies the Laplace equation. The above equation has different forms in different coordinate systems. For example, using spherical coordinate system it can be expressed as

$$\boldsymbol{\frac{1}{r^2} \frac{\partial}{\partial r} \left(r^2 \frac{\partial v}{\partial r} \right) + \frac{1}{r^2 sin\theta} \frac{\partial}{\partial \theta} \left(sin\theta \frac{\partial v}{\partial \theta} \right) + \frac{1}{r^2 sin^2 \vartheta} \frac{\partial^2 v}{\partial \emptyset^2} = 0} \qquad (\mathbf{2.56})$$

Practically, the DC resistivity survey is conducted with two current electrodes (AB) called source and sink in which the current I (A) is injected in to the ground and two potential electrodes (MN)

where the potential difference ΔV (V) is recorded. If we consider (DC) source which delivers current I (A) to the homogenous, isotropic earth through the current electrodes, the potential at any point will vary as a function of r where r is the distance from the ground to the current electrodes. Figure 2.5 shows the arrangement of current and potential electrodes, current lines and equipotential surfaces in a homogenous isotropic ground when the direct current source is. Used

Assuming that the air above the ground has zero conductivity, the Laplace equation in spherical coordinate system which is used to find the relation between the potential at r distance from the current electrode so that equation (2.56) can be reduced to

$$\nabla^2 V = \frac{d^2V}{dr^2} + \frac{2dV}{rdr} = 0 \qquad (2.57)$$

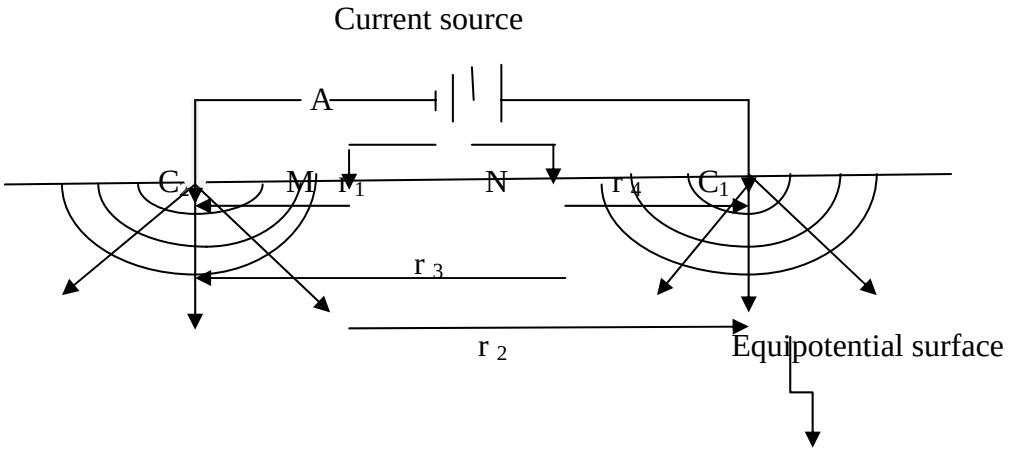

Figure 2.5 Diagram showing the arrangement of current and potential electrode in a four electrode system

Since the potential varies only as function of r,$\frac{\partial v}{\partial \emptyset}$ and$\partial V/\partial\theta$ will become zero

Multiplying equation (2.57) throughout by r^2 it will become

$$r^2\frac{d^2v}{dr^2}+2r\frac{dv}{dr}=0 \qquad (2.58)$$

Integrating both side of this equation gives

$$V=-\frac{C1}{r}+c2 \qquad (2.59)$$

where C1 and C2 are integration constants to be solved by using the following boundary conditions.

Boundary condition (i) $V\rightarrow 0\ as\ r\rightarrow\infty$ then C_2=0

Boundary condition (ii) $\frac{dv}{dz}=o \quad at\ z=o$

Boundary condition (iii) the current flows through a hemispherical surface in the lower half, so that $I=2\pi r^2 J$ but $J=\sigma E=-\sigma\frac{dV}{dr}$ and $\frac{dv}{dr}=\frac{C1}{r^2}$ but $J=-\sigma\frac{C1}{r^2}$

substituting this in to equation (2.59)

$I=2\pi\sigma C_1$ or $C1=-\frac{I\rho}{2\pi}$, where ρ and σ are resistivity and conductivity of homogenous isotropic ground respectively.

Therefore equation (2.59) can be written as

$$V=\frac{I\rho}{2\pi}\left(\frac{1}{r}\right) or \qquad \rho=2\pi r\left(\frac{v}{r}\right) \qquad (2.60)$$

When the distance between the two current electrodes is finite, the potential at any nearby point will be affected by both current electrodes. Therefore, the potential at N due to C1 is

$V_1=\frac{I\rho}{2\pi}(\frac{1}{r1})$ and due to C_2 at N is $V_2=-\frac{I\rho}{2\pi}(\frac{1}{r_2})$ because the current at the two electrodes are equal in magnitude but opposite in sign.

The total potential at N is given by

$$\boldsymbol{V_N = \frac{I\rho}{2\pi}\left(\frac{1}{r1} - \frac{1}{r2}\right)} \qquad (\mathbf{2.61})$$

Similarly the potential at M due to C_1 and C_2 is

$$\boldsymbol{V_M = \frac{I\rho}{2\pi}\left(\frac{1}{r3} - \frac{1}{r4}\right)} \qquad (\mathbf{2.62})$$

The potential difference (pd) measured between the potential electrodes is

$$\boldsymbol{\Delta V = V_N - V_M = \frac{I\rho}{2\pi}\left(\frac{1}{r1} - \frac{1}{r2} - \frac{1}{r3} + \frac{1}{r4}\right)} \qquad (\mathbf{2.63})$$

where r_1, r_2, r_3 and r_4 are all in meters.

Therefore, after re-arranging the distances between the current and potential electrodes according to well known configurations we can determine the resistivity of homogeneous ground

2.3.3 Apparent Resistivity

If the ground is homogeneous, the potential difference measured is a function of true resistivity of homogenous earth and the geometrical factor. But in reality the ground is locally in homogeneous and the potential difference measured depends on current applied ,the resistivity of subsurface medium and geometrical factor(K) determined by electrode array of configurations types .The resistivity calculated from such non-homogeneous ground is not true resistivity rather it is called apparent resistivity (ρa) which can be related to the parameters as

$$\rho_a = K\frac{\Delta V}{I} \qquad (2.64)$$

This apparent resistivity has to be interpreted using either curve matching or inversion techniques to find the estimated resistivity versus depth of the subsurface.

There are many types of electrode configuration used in ground surveys, of which the most commonly used array are Wenner, Schlumbereger and dipole-dipole. Since the electrode separation relates to the investigation depth and lateral resolution power required, one can choose the best electrode configuration for his planed survey at the very beginning of his survey .The expression for apparent resistivity in each of the above array types will be different due to the difference in geometrical factor (K) of each array types.

Let us consider the schlumberger array in which the electrodes are symmetrical placed at appoint at the center of array as shown in Figure 2.6

where r_1=s-b, r_2=s+b, r_3=s+ b and r_4=s-b and 'O' is the center of the array.

The potential difference ΔV using equation (2.63) is given by

$$\Delta \boldsymbol{V} = \frac{\boldsymbol{I\rho}}{\boldsymbol{2\pi}}\left(\frac{\boldsymbol{2b}}{\boldsymbol{S^2 - b^2}}\right) \qquad (\mathbf{2.65})$$

And ρ_a is given by

$$\boldsymbol{\rho_a} = \boldsymbol{\pi}\left(\frac{\boldsymbol{S^2-b^2}}{\boldsymbol{2b}}\right)\left(\frac{\boldsymbol{\Delta V}}{\boldsymbol{I}}\right) \qquad (\mathbf{2.66})$$

where the geometrical factor K= $\pi\left(\frac{S^2-b^2}{2b}\right)$ and it is different for different arrays.

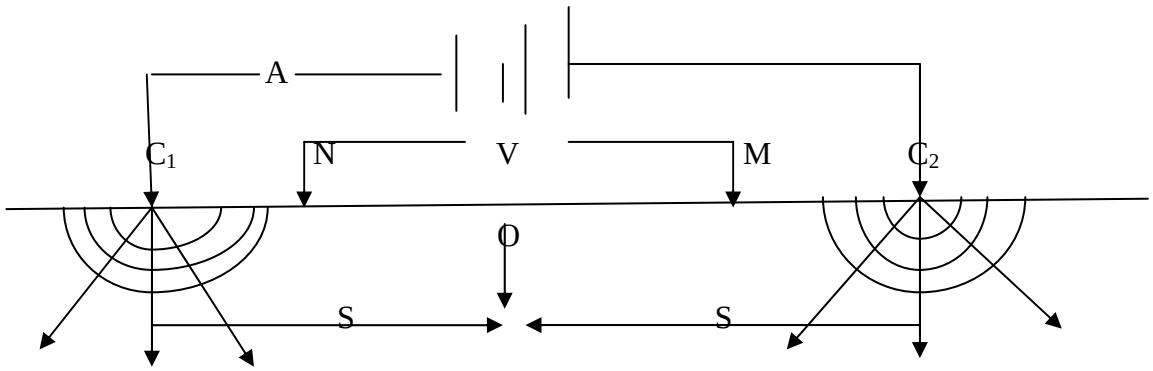

Figure 2.6 the electrode arrangement of Schlumberger array.

In addition to the array types, one will choose the appropriate resistivity survey procedures depending on the objective of the study. Some of the most commonly used procedures in resistivity surveying work are resistivity profiling, resistivity soundings and electrical surface imaging. Depending on the specific objectives and the geology of the area, one can use profiling mainly to obtain information on lateral variations in resistivity, resistivity sounding to determine the variation in resistivity in the vertical direction of horizontally stratified layer earth or electrical surface imaging which combines surface profiling with vertical soundings using a multi-electrode array to produce two dimensional (2D) or three dimensional (3D) images of the subsurface.

2.3.4 Vertical Electric sounding

Vertical electrical sounding (VES) consists of a symmetrical electrode array used to determine the resistivity of the subsurface which is assumed to be horizontally stratified layers. The procedure is used to determine the variations in resistivity in the vertical direction and called electrical drilling or commonly vertical electrical sounding (VES). By expanding symmetrically the distance between current electrodes about a point called the sounding point, while keeping the potential electrodes MN at the same position, provides a sounding curve corresponding to the apparent resistivity versus depth of the location. As the spacing between the current electrodes increases, the investigated depth will also increase .The two most commonly used arrays in

electrical sounding survey are the Wenner and Schlumberger arrays. In this work, we have used the data which was collected by using the Schlumberger electrode array techniques. When the Schlumberger array is used, the distance between the potential electrodes is not greater than one tenth of the current electrodes spacing. The advantage of this array is that initially only the spacing between the current electrodes is increased. However, at large current electrode spacing, the measured potential becomes very low and the distance between the potential electrodes is increased. Increasing the potential electrode spacing produces a 'step' in the apparent resistivity curve and it is good practice to obtain an overlap between the curve segments by obtaining two readings at different potential electrode spacing for two adjacent current electrode spacing. Segments obtained at larger potential electrode spacing can be shifted in order to produce a smooth curve (Gibson and George, 2003).

CHAPTER 3

DATA ANALYSIS AND PROCESSING

3.1 General

The data used for this work is a secondary data, which is the property of the Oromia Water Works Design and Supervision Enterprises (OWWSDE). The data is received at the stage where the temporal correction are already been carried out.

Based on the criteria selection of Oromia Water Works Design and Supervision Enterprises (OWWSDE), the Wobok-Dilo area is one of the areas selected to be studied using integrated geophysical methods for the sake of exploring the groundwater potential of the area based on previous detailed geological and reconnaissance geophysical surveys. This area is selected for detailed study to understand the different lithologic units, groundwater potential zones, geological structures and physical properties of subsurface rocks using a combination of geophysical techniques namely, resistivity and gravity methods of prospecting.

3.2 Resistivity Data processing

The resistivity survey was conducted along six survey lines oriented approximately EW,NS and partially NNE with in the area .Total of twenty one vertical electrical sounding points (VES) along six different survey lines, using Schlumberger configuration with AB/2 spacing ranging from 1.5m to 1000m, were surveyed in the study area. Some of the VES namely VES8, VES7 and VES4 were surveyed near previously drilled borehole. Figure 3.1 shows the location of VES points and the drilled borehole to assist parameterization of resistivity result.

First the raw resistivity data which were entered in to excel sheet was prepared for other software and the apparent resistivity pseudodepth section along profiles and the apparent resistivity sliced pseudodepth map of the whole area for different current electrode spacing were prepared by using surfer9 software. The one dimensional (1D) molding of VES data was done by using resistivity modeling software called Resix-IP and WinResist. The depth and resistivity of subsurface rocks beneath VES points were determined from the one dimensional inversion of

VES data .The parameters from the modeled VES (resistivity and depth) are used to make the geoelectric sections along two survey lines (Line-6 & 1) by using AutoCAD drawing software and later modified by Sulfer9 software.

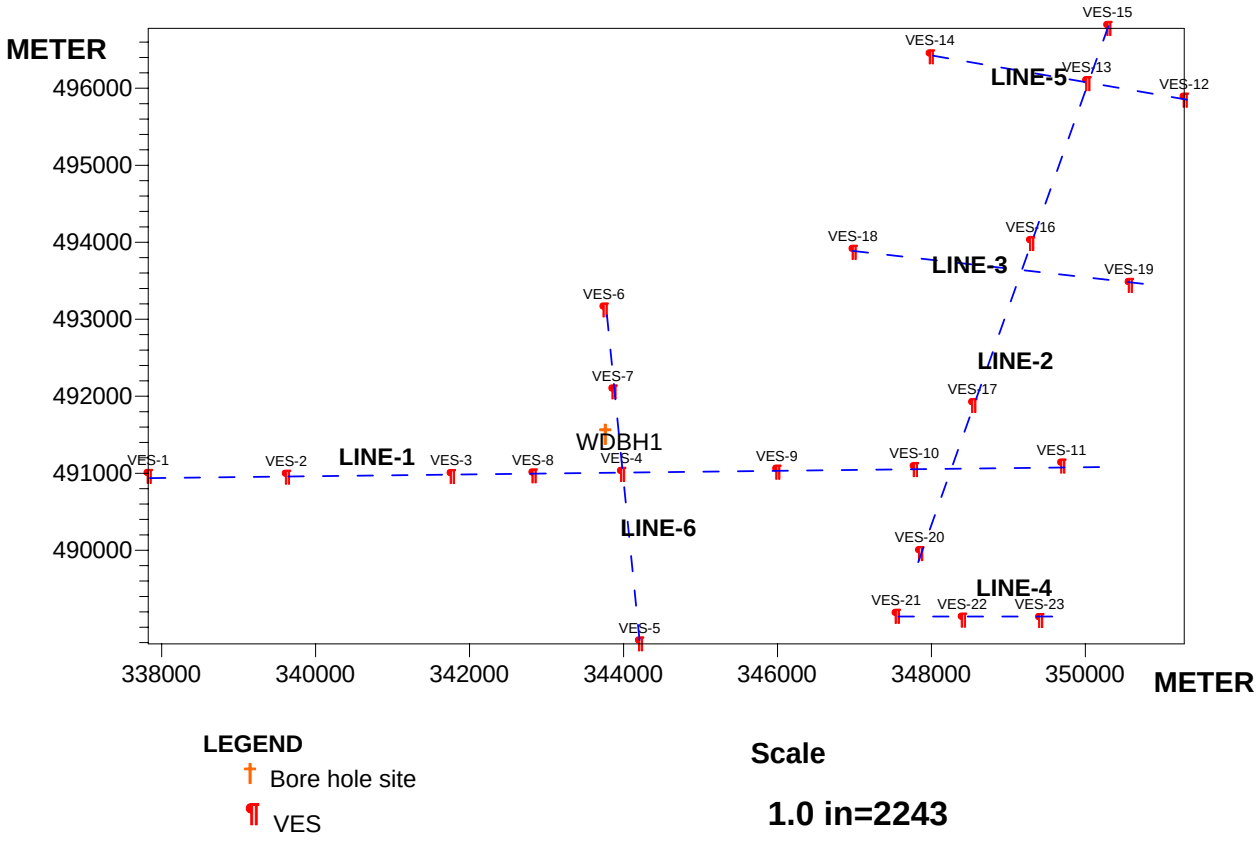

Figure 3.1 Location of the vertical electrical sounding (VES) points and Borehole

3.3 Ambiguities of Sounding Curve Interpretation

The Vertical Electrical Sounding curve modeling and interpretation is linked to the principle of equivalence. The principle expresses that a measured sounding curve is basically related with many physically equivalent models that may differ considerably. The VES data can be interpreted with different number of layers without any preference. Another important property

of vertical electrical sounding curves is evident. By all appearances, only the minimum number of layers can be deduced implying that thin layers are preferentially suppressed. A rule of thumb indicates that a layer becomes clearly visible in a sounding curve if its thickness is comparable to its depth of deposition (Kirsch, 2006).

To avoid the ambiguity of equivalence in the 1D inversion of VES data and check the continuity of layers in the area, the data of one borehole (WDBH1) was used to fix the model parameters and attempt is made to get depths independent of equivalence for L6-V4, L6-V7, L1-V8 and L1-V4. Once the resistivity and depth for the above mentioned VES were determined by fixing their depth from the boreholes (lithology data) using ResixIP software, the depth and resistivity of the other VES along these survey lines were estimated by using the information from borehole. The resistivity parameters which were estimated form constrained and parameterized 1D inversion of VES data using ResixIP software, were used as initial model for WinResist software to find the final resistivity layer parameters. The software WinResist uses iterations techniques to adjust the fitting between the observed data curve and the initial model parameters. Several reinterpretations for modeled soundings curves were performed to get better model parameters and the iteration process was finalized when the root mean square (RMS) errors was less than 5%.

3.4 Gravity Data processing

A total of one hundred three (103) measured gravity points have been used to cover the study area. The distance between neighboring gravity stations ranges between 300 to 500 meters along profiles, and 800 to 1000 for some infill stations between the survey lines. The data points are given in Figure 3.2.

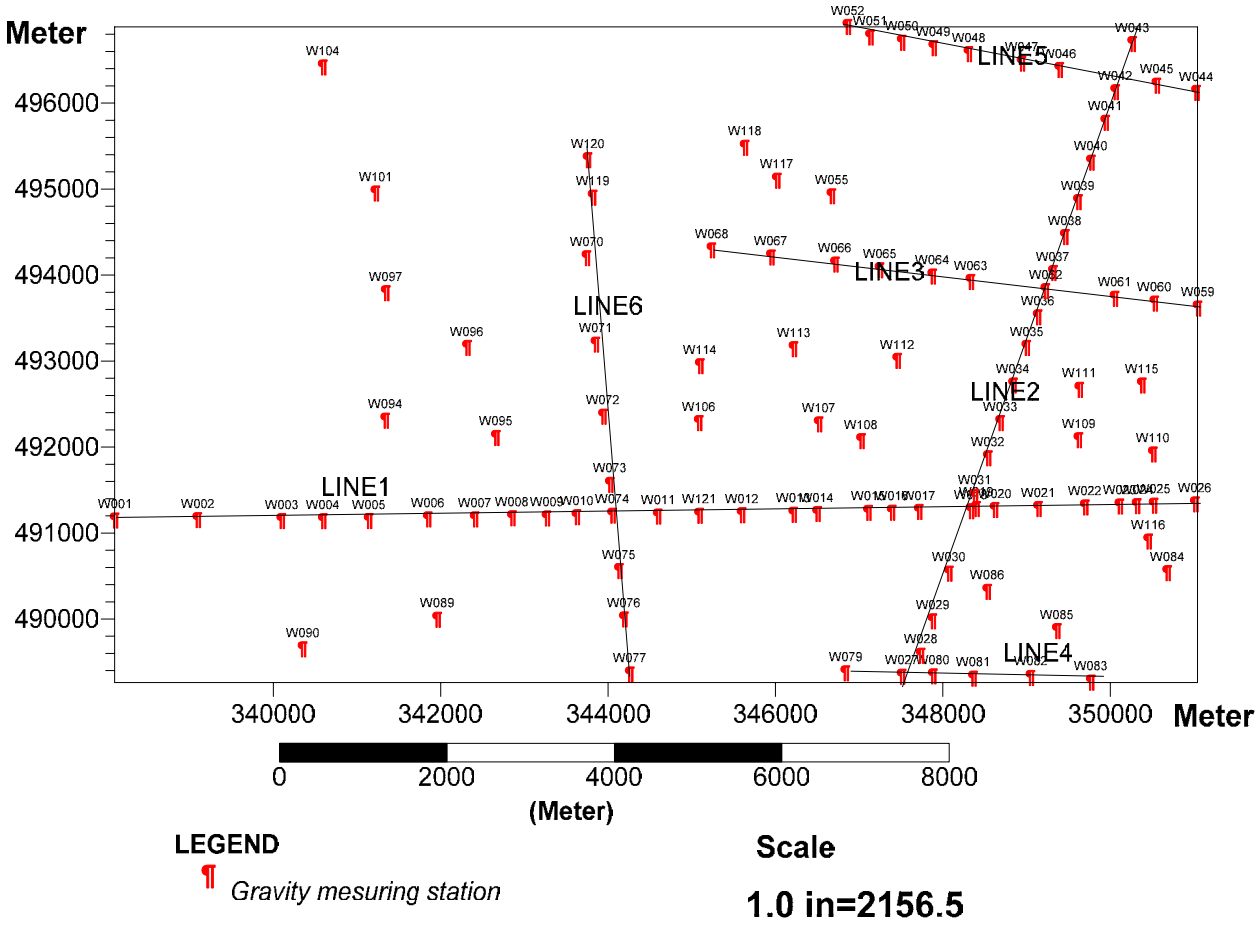

Figure 3.2 Gravity measuring stations.

The raw gravity data (corrected for temporal variations) were then corrected for spatial variations such as atmospheric effects, Freeair and intermediate layer reductions using the software GRAVRED (Elias Lewi, 1997) to yield the Freeair and Bouguer anomalies respectively. A density value of 2.67 g/cm^3 (which is the average density of crustal rocks) was used for intermediate layer reduction. The Bouguer anomaly generated was simple Bouguer anomaly since the terrain reduction was not carried out. This is because the area has not as such rugged topography. It is also believed that the gently varying topography would have a linearly varying effect that can be filtered easily. Therefore, it is preferred to filter possible linear terrain effect using data filtering techniques. The simple Bouguer anomaly was then further processed to separate the residual from the regional effects to come upon with the residual and regional anomalies. This was necessary not only to remove unaccounted linear effect during data

reduction but also to separate short wavelength gravity effect(due to shallow structures which is important for this work) from long wavelength gravity effects (due to deep seated structures). For this work, both first and second order polynomial surface were fitted to the simple Bouguer anomaly using the program POLFIT (Elias Lewi, 1997) and the fitted surface was considered as the regional anomaly while the difference between the Bouguer anomaly and fitted data was taken as the residual anomaly. Finally, the mapping software called Surfer9 was used to obtain different anomaly maps and modeling software called GravMag was used to model the subsurface using the residual anomaly along one profile.

3.5 Reliability of Gravity Reduction

The raw gravity value and height are negatively correlated with the square of the Pearson correlation coefficient being 0.795. As one can see from Figure 3.3, the regression using the least square approach showed that 79.5% of the raw gravity value is explained by the height. This strong negative correlation of raw gravity value with elevation is also expected .Here it should be noted that, the raw gravity data does not mean the gravity data that is collected from the field but the gravity data that is corrected for drift, tide, pressure and that reduced to the surface of ground.

Even though the free-air correction (Figure 3.4) has reduced the correlation between the gravity anomaly and the height, 40.3% of it is still being accounted for the height .That means only 39.2% correlation in the raw gravity was removed. From theoretical point of view also this positive correlation is to be expected after the free-air reduction.

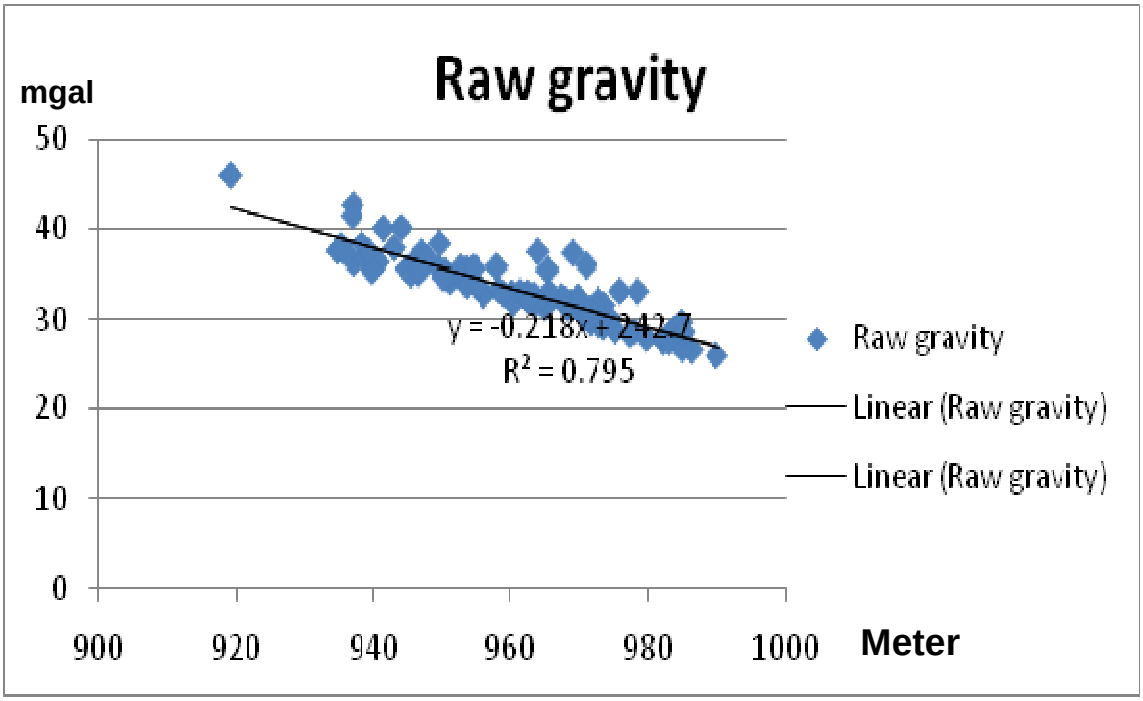

Figure 3.3 Graph of raw gravity versus height.

.

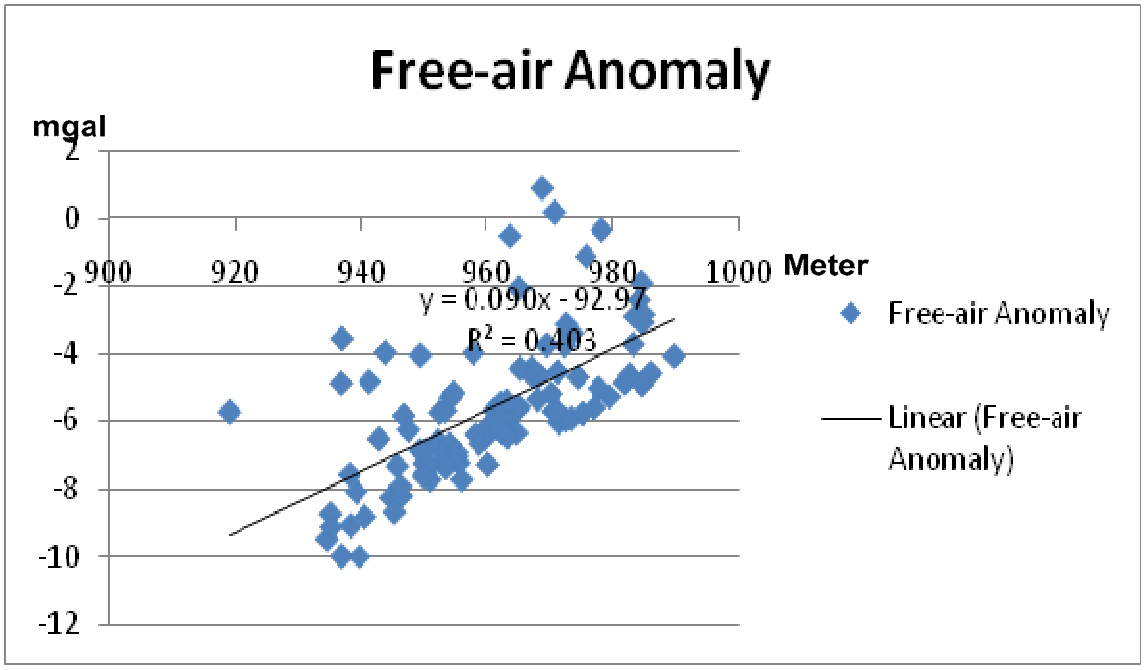

Figure 3.4 Free-air Anomaly versus height.

The Bouguer anomaly has less correlation with height. Figure 3.5 shows the square of the linear correlation coefficient between the two values is 0.03.The correlation observed in the raw gravity (79.5%) or in the free air anomaly (40.3%) with height are removed in the case of simple Bouguer anomaly. As it was explained in the 3.3. Gravity data processing subtopic, the value of the density used for the intermediate layer reduction was 2.67g/cm3, which is the average density of crustal rocks. When one analyzes this small correlation value of 0.03 from the perspective correlation analysis, it is negligible. Therefore one can with certainty of the 3% start data interpretation.

.

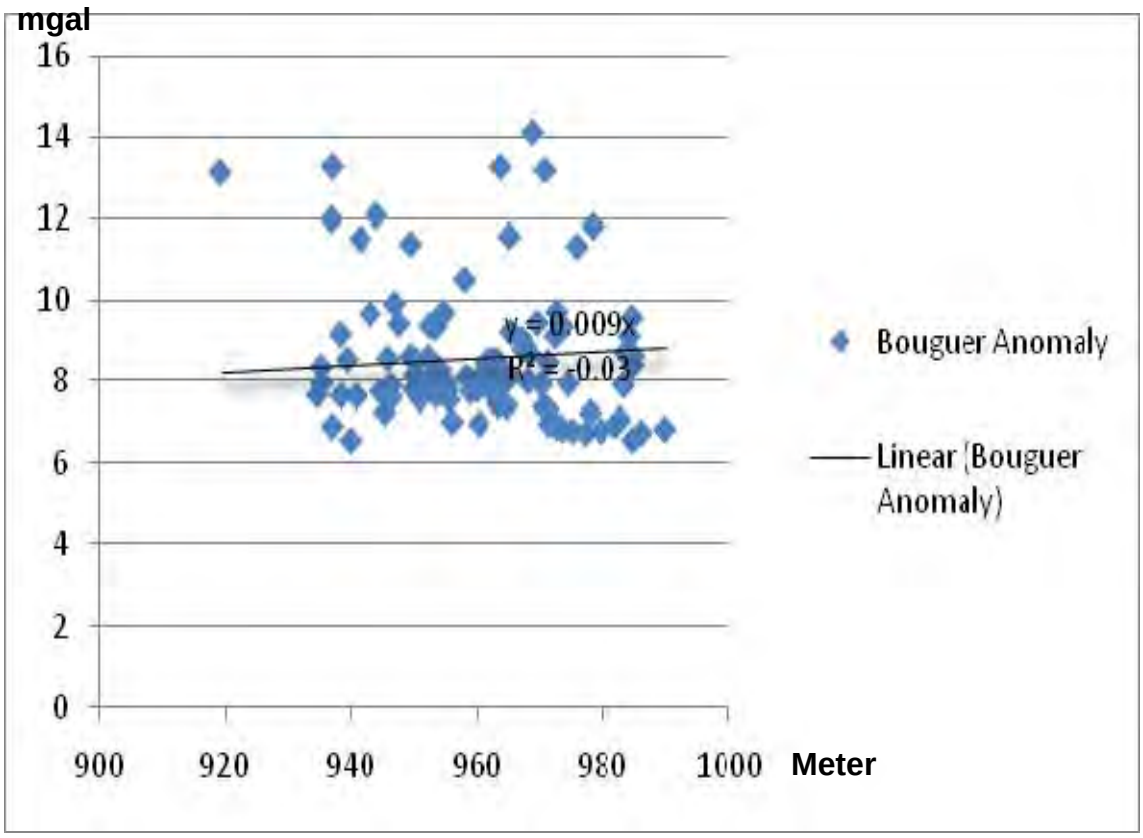

Figure 3.5 Bouguer Anomaly versus height

CHAPTER 4

RESULT, DISCUSSION AND INTERPRETATION

4.1 Result and Discussion of Different Anomaly Maps

The results of the geophysical data were used to produce different anomaly maps which show contrast in the resistivity and density of the subsurface rocks. In this work the VES and gravity data were used to produce maps and examine the relative contrast in resistivity and density of the subsurface rocks. In order to study the contrasts in resistivity and density of the subsurface rocks; plots of pseudodepth sections and gravity profiles (second degree residual gravity anomaly versus distance) along two survey lines, apparent resistivity sliced pseudodepth map of the study area for six current electrode spacing, free-air, Bouguer, residual and regional gravity anomaly maps were prepared and presented in this section.

4.1.1 Apparent Resistivity Maps and Gravity profiles

The apparent resistivity data of different VES at current electrode spacing AB/2=9 is taken to produce the apparent resistivity plane map of the area as shown in (Figure 4.1) .This map shows the apparent resistivity of the area at shallow depth .High apparent resistivity anomaly is observed in the south west, south east and north east of the area, where as low apparent resistivity anomaly is observed in the northern and central part of the area. Very high apparent resistivity value is observed near VES-2, VES-10, VES-20 and VES-16, where as low apparent resistivity is observed nearVES-6, VES-7 and VES-4.

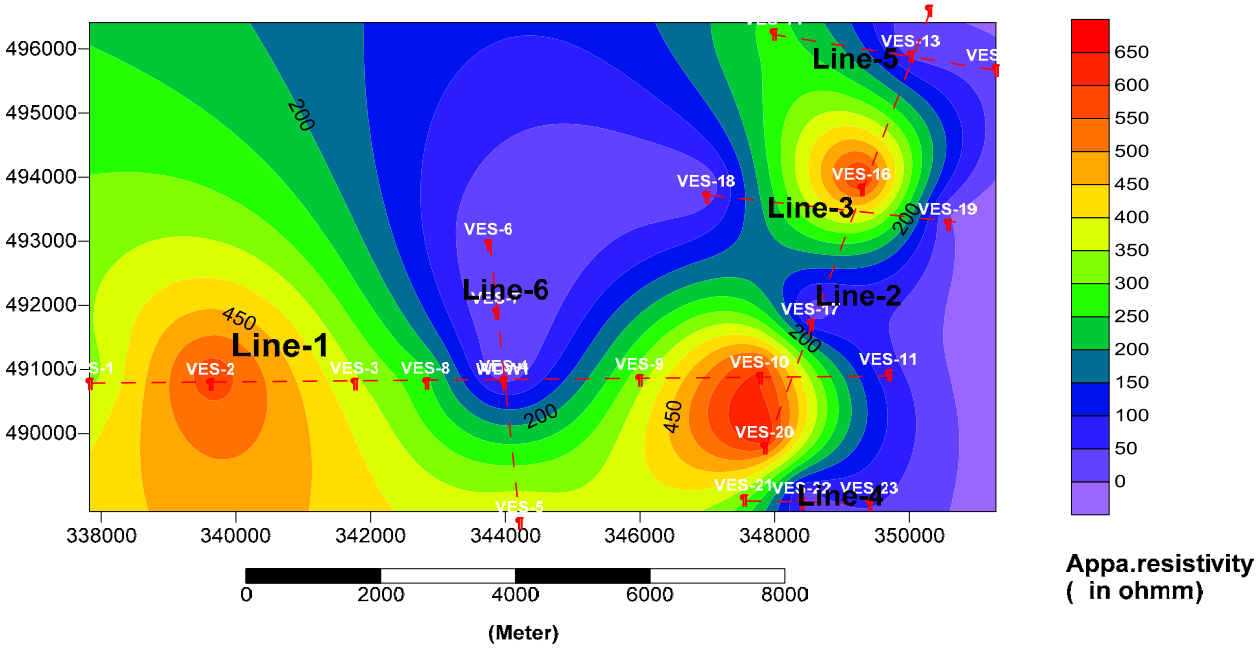

Figure 4.1 Apparent Resistivity plane map for current electrode spacing AB/2=9m.

4.1.2 Apparent resistivity pseudodepth section and residual gravity along survey Line 6

The apparent resistivity pseudodepth section along Line 6 (Figure 4.2) indicates wide variation of apparent resistivity value ranging from 0 to 440Ohm-m.A broader and low apparent resistivity anomalous zone that is dipping toward east with value ranging from 20 to 100Ohm-m is observed beneath VES4. This anomalous zone is extending to VES7 and VES6 at shallow depth. A relatively low apparent resistivity but increasing with pseudodepth is observed beneath VES6. Similar to that of VES4 law apparent resistivity value is observed beneath VES7. A very high apparent resistivity anomalous zone is observed beneath VES5 up to pseudodepth 750m but decreasing its magnitude below pseudodepth of 750m.The gravity profile along this survey line shows the variation of second degree residual anomaly with distance from west to east. As can

be observed from Figure 4.2 relatively high residual anomaly is observed beneath VES6 and decreases smoothly up VES-7. The residual gravity anomaly attain its lowest value near VES-4 but starting from VES-4 a sharp increment in residual anomaly is observed up to VES-5.

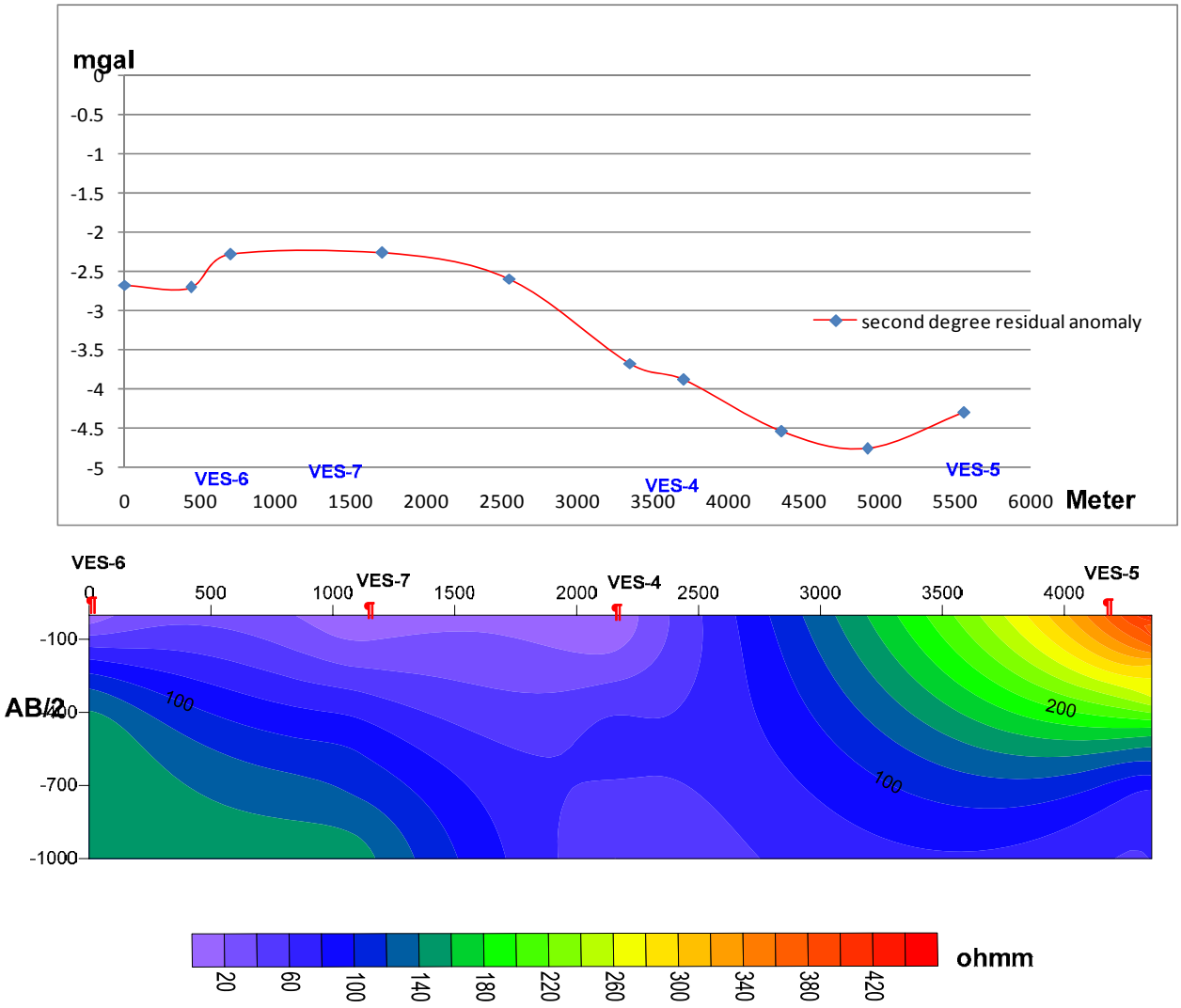

Figure 4.2 Second degree residual anomaly versus distance along profile six and apparent resistivity pseudodepth along Line 6

4.1.3 Apparent resistivity pseudodepth section and residual gravity along survey line one

The apparent resistivity pseudodepth section along Line one Figure 4.3 shows apparent resistivity value ranging from 0 to 800ohm-m which is high in magnitude as compared to that

obtained in survey line six .A very low apparent resistivity is observed beneath VES-4 and very high apparent resistivity is observed beneath VES-2 and VES-10.

The second degree residual gravity anomaly along this survey line ,the top parts (Figure 4.3) shows a maximum value of residual anomaly over VES-2 and drastically decreases and attain its lowest value between VES3 and VES-4.Starting from VES-4 an increment in residual anomaly is observed and then again reach pick value near VES-10. These drastic changes in the slope is mostly associated with weak zone such as faults. Near VES-11 a slight decrement in gravity anomaly is observed relative to that of VES-10.

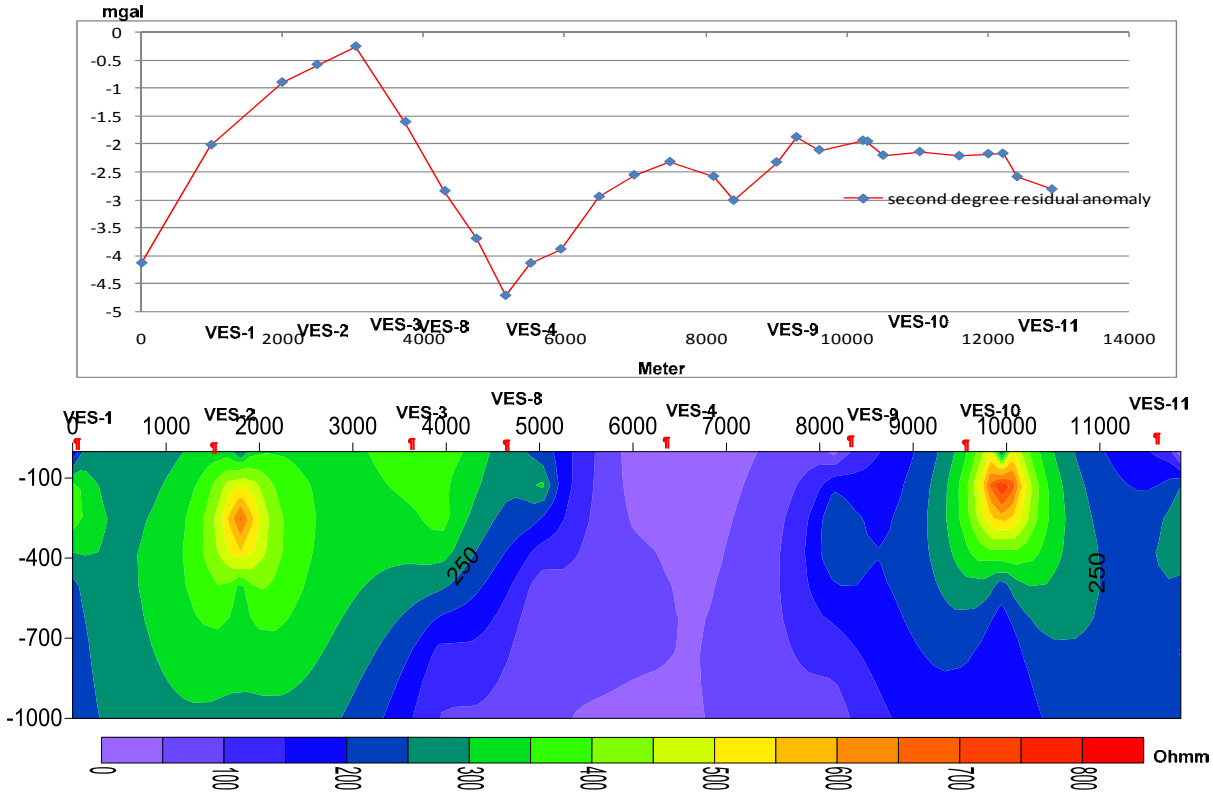

Figure 4.3 Second degree residual anomaly versus distance along profile one and apparent resistivity pseudodepth section

4.1.4 Apparent resistivity sliced pseudodepth map

The apparent resistivity sliced Pseudodepth map (Figure 4.4) was prepared by superimposing the two dimensional apparent resistivity plan maps for six different current electrode spacing. This map shows the relative variation of the apparent resistivity value of the whole area laterally as

well as vertically at different pseudodepths. The apparent resistivity value varies from 1-1300Ohm-m. The amplitude of the high apparent resistivity value zone, which is observed in western part, decrease as the investigation depth increase. The amplitude of the very low apparent resistivity zones which was observed in the northern and central parts of the area (Figure 4.1) increases as depth increase. High apparent resistivity value which is observed in the eastern and south eastern part of the area starts to increase both in magnitude and amplitude up to pseudodepth of 45m and then start to decrease both in magnitude and amplitude up to pseudodepth of 1000m .Similarly high apparent resistivity value which is observed in the western corner of the area starts to decrease in value up to pseudodepth of 45m and increase in magnitude and amplitude up to pseudo depth of 100m and then finally starts to decrease in its value up to pseudodepth of 1000m.

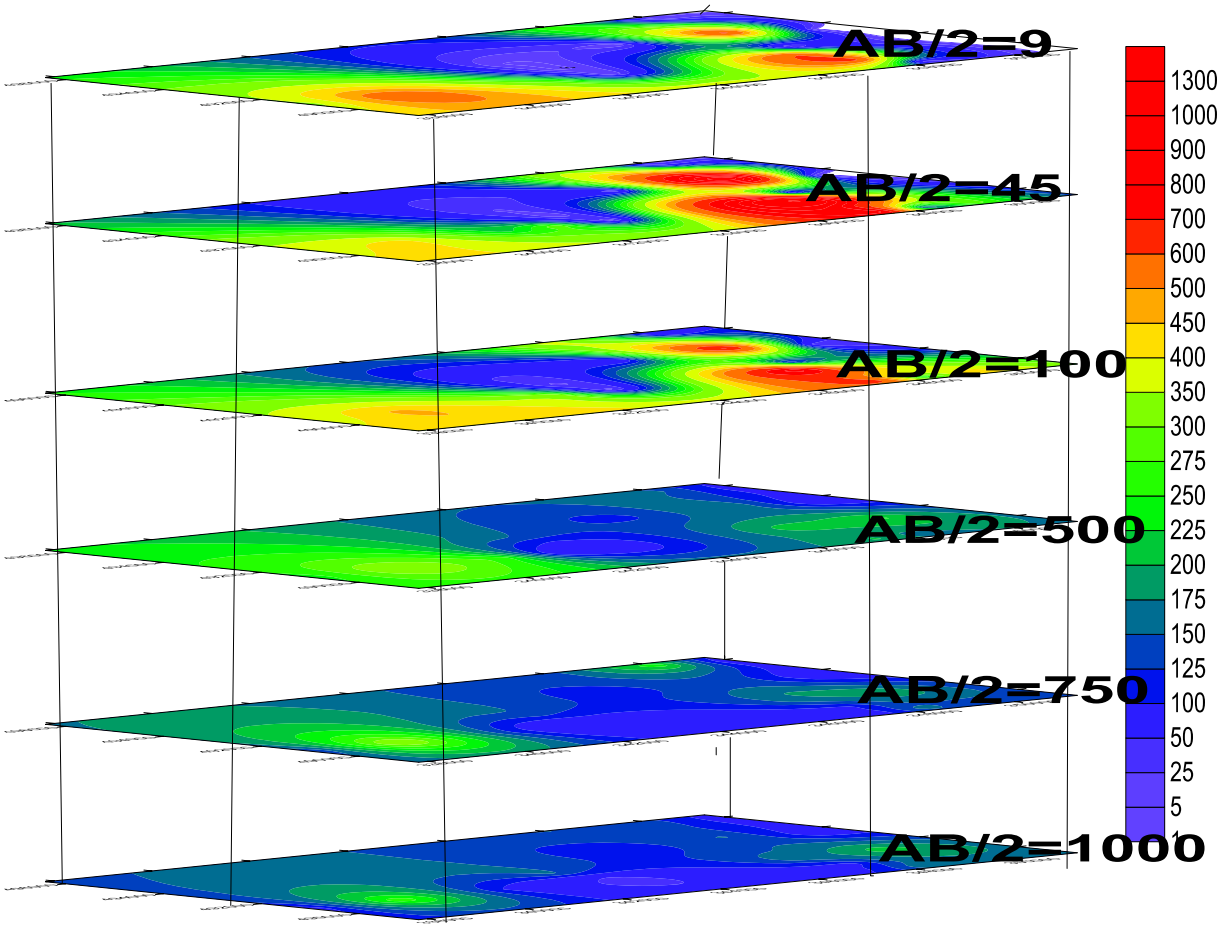

Figure 4.4 apparent resistivity sliced pseudodepth map

4.2 Gravity Anomaly maps

4.2.1 Free-Air anomaly and topography map

Figure 4.5 shows the topography of the survey area and Figure 4.6 the free-air anomaly. The value of the free-air anomaly varies between -12mgal to -0.5mgal whereas the height of the area varies between 920m to 990 m in reference to WGS84 reference ellipsoid. The free-air anomaly map was plotted with a contour interval of 0.5mgal and the topography map with 5m contour interval by using surfer9 mapping software. As stated in chapter 3 the free –air anomaly (mgal) and elevation in (meters) have appositive correlation with correlation coefficient of 0.43. Figure 4.5 and 4.6 shows the relative variation of Free-air and topography values in the study area .The minimum value of free- air anomaly was observed in the south, south-eastern part of area where as the maximum value of free-air anomaly was observed in the south- western part of area. The topography of the study area has minimum value near south-western part of the area and maximum value near north- eastern part of area. The free – air anomaly has a strong positive correlation with elevation, which is also expected theoretically.

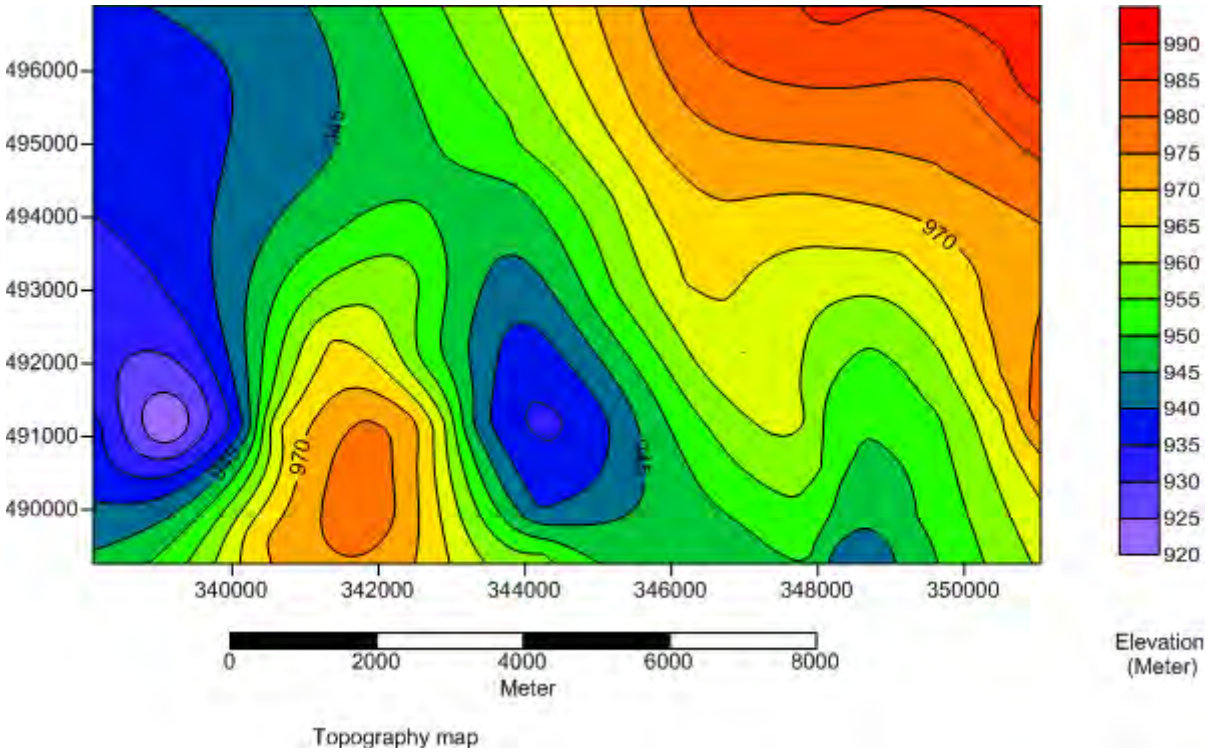

Figure 4.5 Topography map.

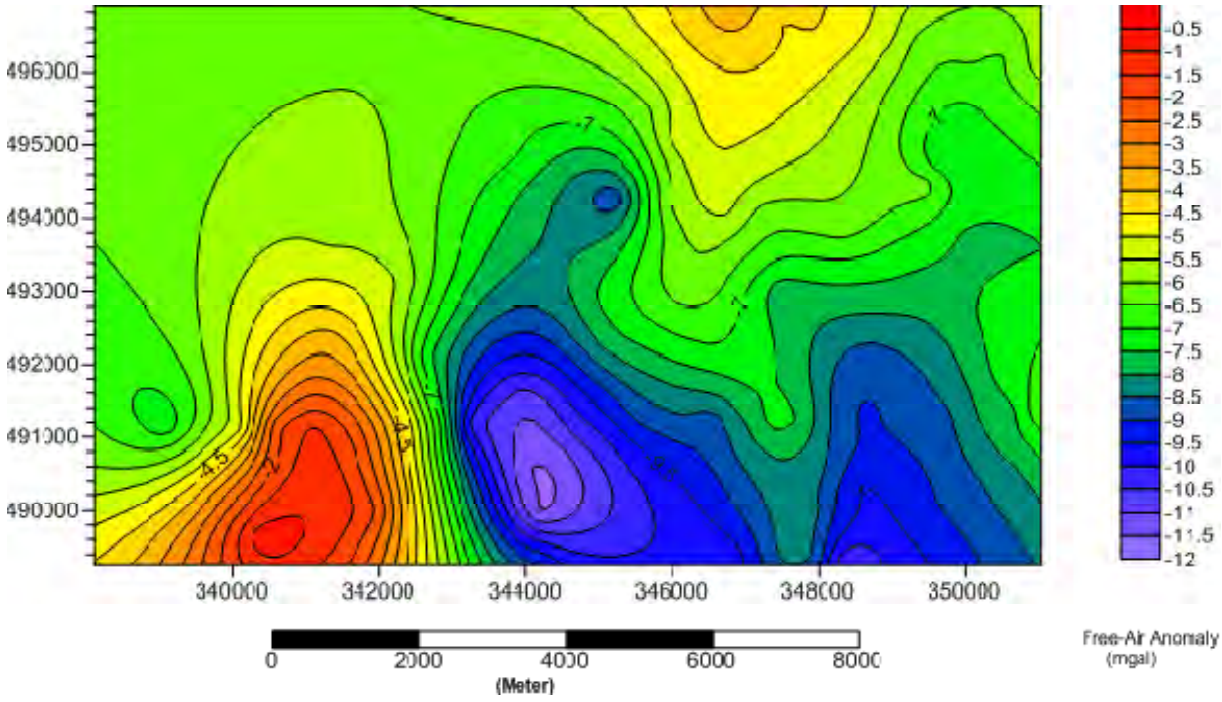

Figure 4.6 Free-air Anomaly map.

4.2.2 Bouguer Anomaly Map

The Bouguer anomaly of the study area Figure 4.7 is the result of Bouguer reduction in which the topographic effect was minimized .It has a contour interval of 0.5mgal and its value varies from 4.5 to 13.5mgl.The law Bouguer anomaly value (4.5 to 7mgal) is observed in the eastern, north eastern and south eastern part where as the high Bouguer anomaly value (10.5 to13.5mgal) is observed in the south- western and northern part of area. The high free-air anomaly value which is observed in the south western part of the area is also seen in Bouguer anomaly. It has similar trends with that of free-air anomaly. The law Bouguer anomaly value in the east, north-eastern, south and south-eastern parts of the area is seen as medium value in free-air anomaly. This shows that, the medium value in free-air anomaly is affected by medium topographic effect and the related Bouguer plate.

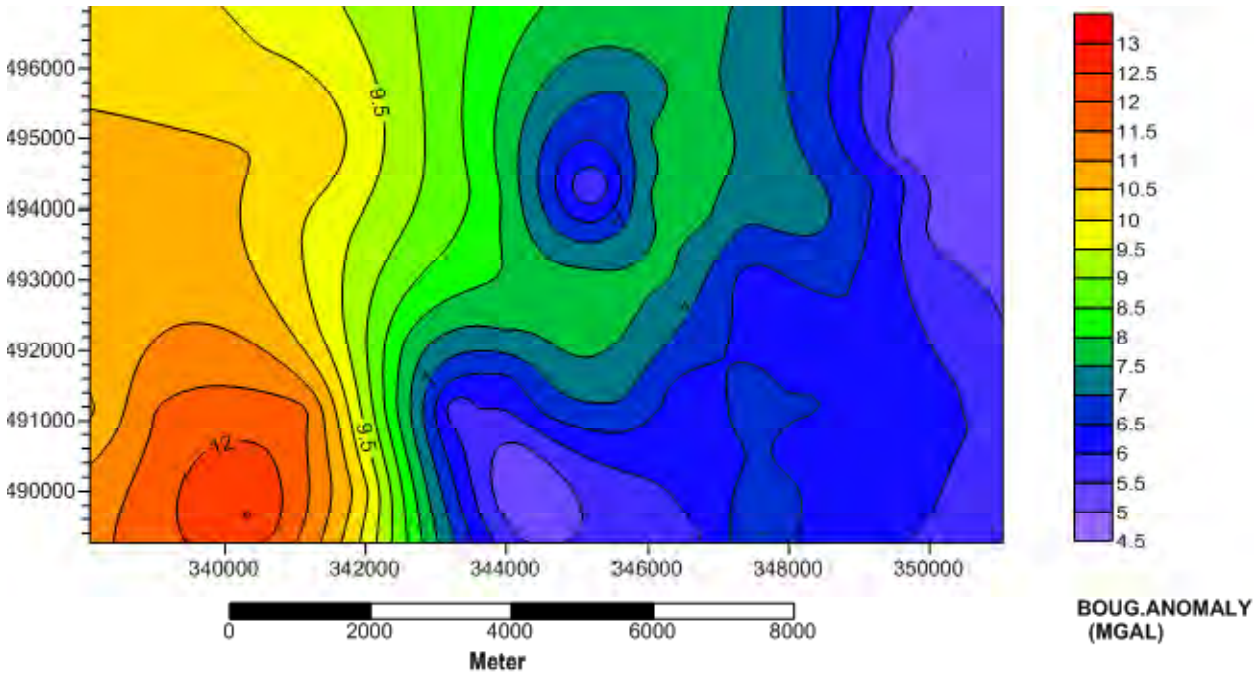

Figure 4.7Bouguer Anomaly map

4.2.3 Residual Gravity Anomaly Maps

The residual gravity anomaly given in Figure 4.8 and 4.9 were produced by fitting first and second degree polynomial to the Bouguer anomaly data respectively. The first degree residual gravity anomaly has a contour interval of 0.4mgal and its value varies from -2.8 to 3.2mgal. It has lowest value in the central north and south central part of the area. The maximum value in the south western part of the area is also observed in the Bouguer anomaly with little modification in their relative value but with the same trend. This shows the very high anomaly zone in the Bouguer anomaly map is less affected by the compensational signal effects relative to east, north-east and south-east of the area

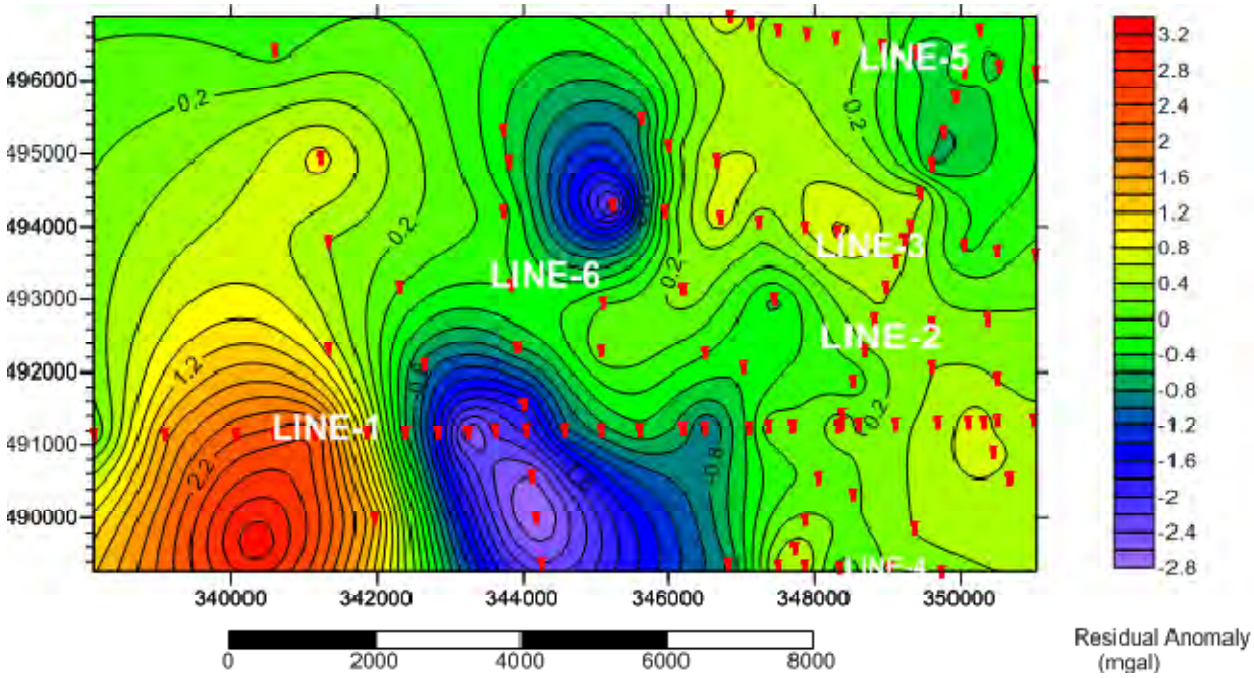

Figure 4.8 First degree polynomial surfaces fitting residual anomaly map

The second degree residual gravity anomaly map (Figure 4.9) has a contour interval of 0.2mgal and its value varies from -4.8 to 0.6mgal .It has very low anomaly zone near line one of VES4, VES8 and line 6 of VES6. Similar to Bouguer anomaly high residual anomaly is observed

beneath line one of VES2 and VES3 i.e in the western part of the area, which is also observed in the Bouguer and first degree residual anomaly maps with little modification in their size , shape and amplitude but with the same trends. This shows that this high anomaly zone is affected by dense materials underneath. The second degree residual anomaly map near VES18, VES20, VES21, VES22 and VES16 shows medium anomalies value ,where as the Bouguer anomaly map shows low anomaly value .These might be due to the presence of medium dense material underneath at shallow depth.

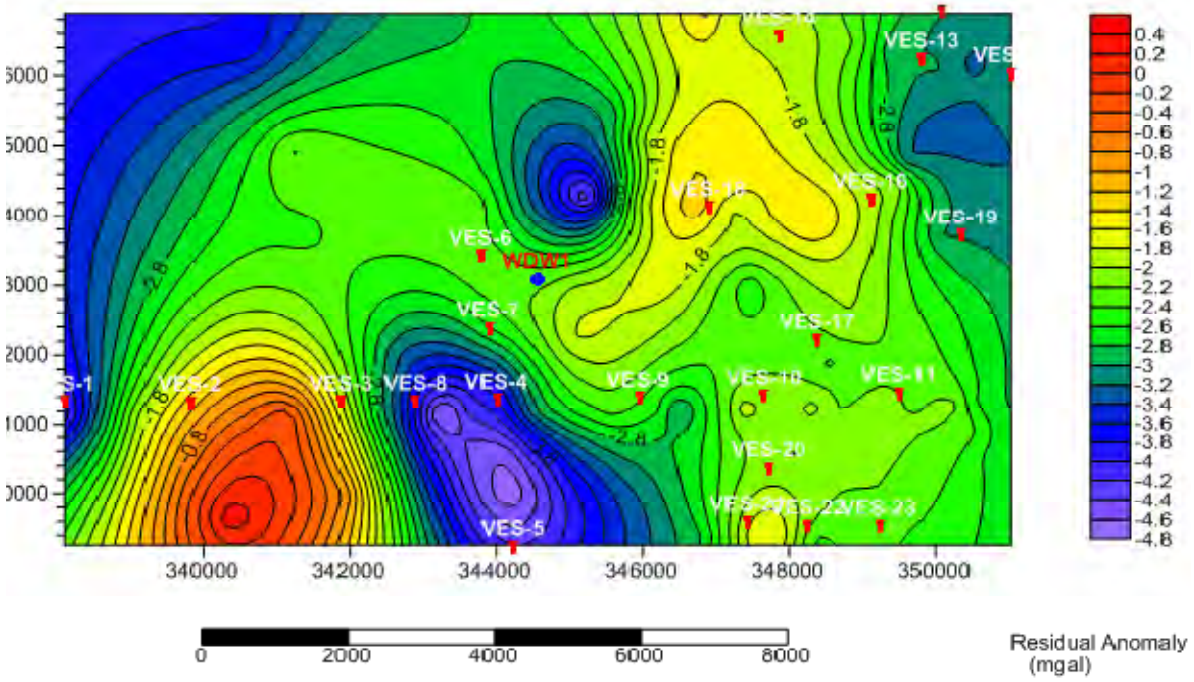

Figure 4.9 second degree polynomial surface fitting residual anomaly map

4.2.4 Regional Gravity Anomaly Maps

The regional anomaly maps (Figure 4.10 and 4.11) were produced by first degree and second degree polynomial surface fitting to the Bouguer anomaly. The first degree regional anomaly

map (Figure4.10) has a contour interval of 0.2mgal and its value varies from 6.8 to12.2mgal .It has low regional anomaly value in the eastern, which is seen as high in topography in the topographic map. Similarly, the high anomaly value in the northern and north western part of the area is reflected as low topography in the topographic map. This clearly indicates that the regional anomaly is the reflection of compensational signal and its effect is removed in the regional-residual separation. Generally, the regional anomaly value increases smoothly from east to west, which is the reverse to topography and the contour line moves from south to north with linear trend.

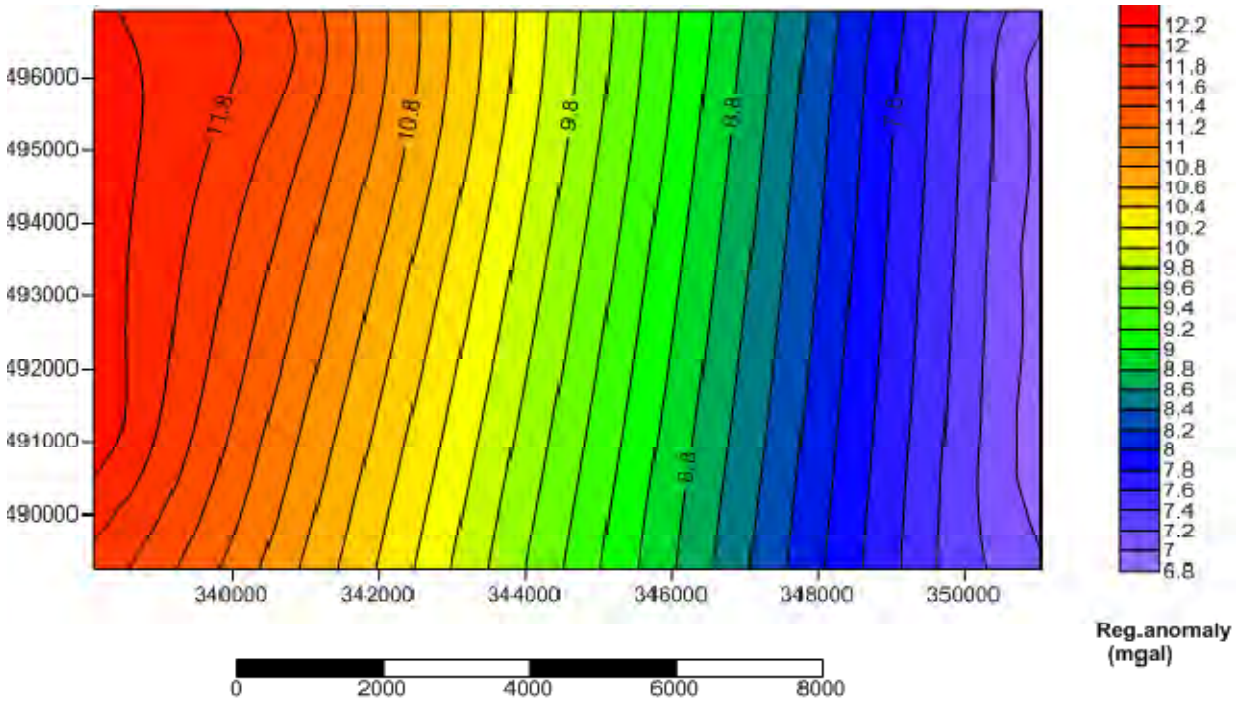

Figure4.10 First degree polynomial surface fitting regional gravity anomaly map

The second degree regional anomaly map (Figure 4.11) has a contour interval of 0.5mgal and range value between 9.5mgal to 16.5mgal .It has low regional anomaly value in the eastern part and highest regional anomaly value in the western part of the area.

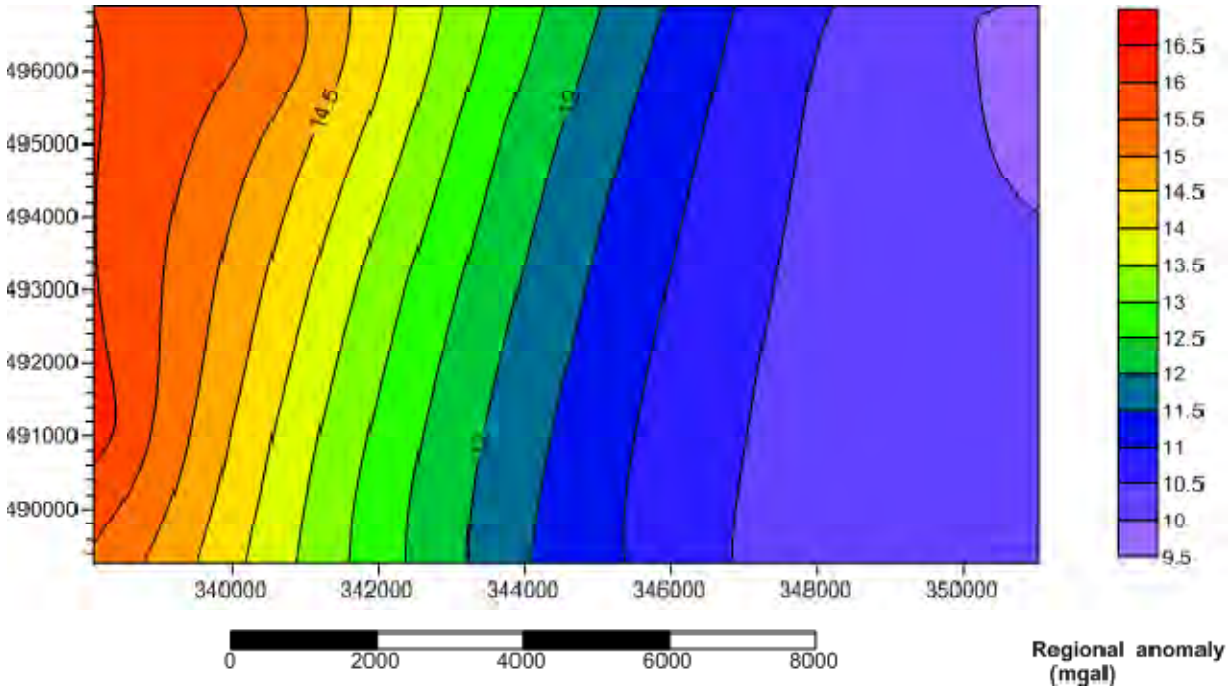

Figure 4.11. The second degree polynomial surface fitting Regional gravity anomaly

4.3 Qualitative Interpretation

For sake of simplicity, names are assigned for three resistive zones shown in apparent resistivity map (Figure 4.1) in order to correlate them with what is observed in the other apparent resistivity and gravity maps.

Zone I .is high apparent resistivity zone in the area, Zone II is low apparent resistivity zones while Zone III is the transition between Zone I and Zone II. Therefore, the interpretation of the region will be made separately in order to have a better picture of them.

Zone I

This high anomaly zone at shallow depth is correlated with the quaternary vesicular basalt. This zone includes areas beneath VES-2, VES-20, VES-10 and VES-16 .The apparent resistivity value of this zone decreases as the depth increase .The decrease in the apparent resistivity of this zone as the depth increase might be due to the weathering and fracturing of the rocks and

possible presence of water saturated zone that overlay the high resistivity basement. The gravity profile along this areas show that the second degree residual gravity anomalies value near VES-2 is high (Figure 4.12b) whereas near VES-20, VES-16 and VES-10 is medium in value. The apparent resistivity for AB/2=1000 remains high beneath VES-2 and the apparent resistivity become low in the remaining areas. Here it should be noted that both maps (Figure 4.12a and Figure 4.12b) reflect the same features.

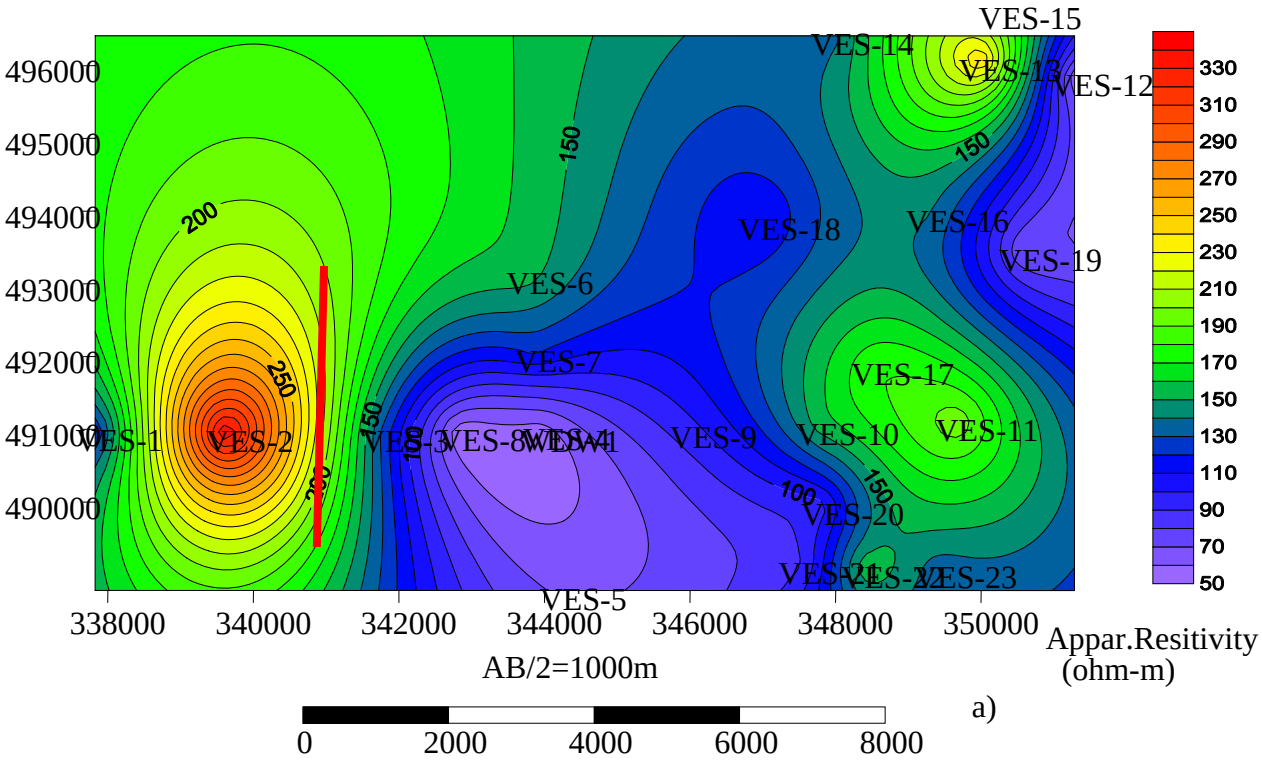

Figure 4.12(a) Apparent resistivity at current electrode separation of AB/2=1000m

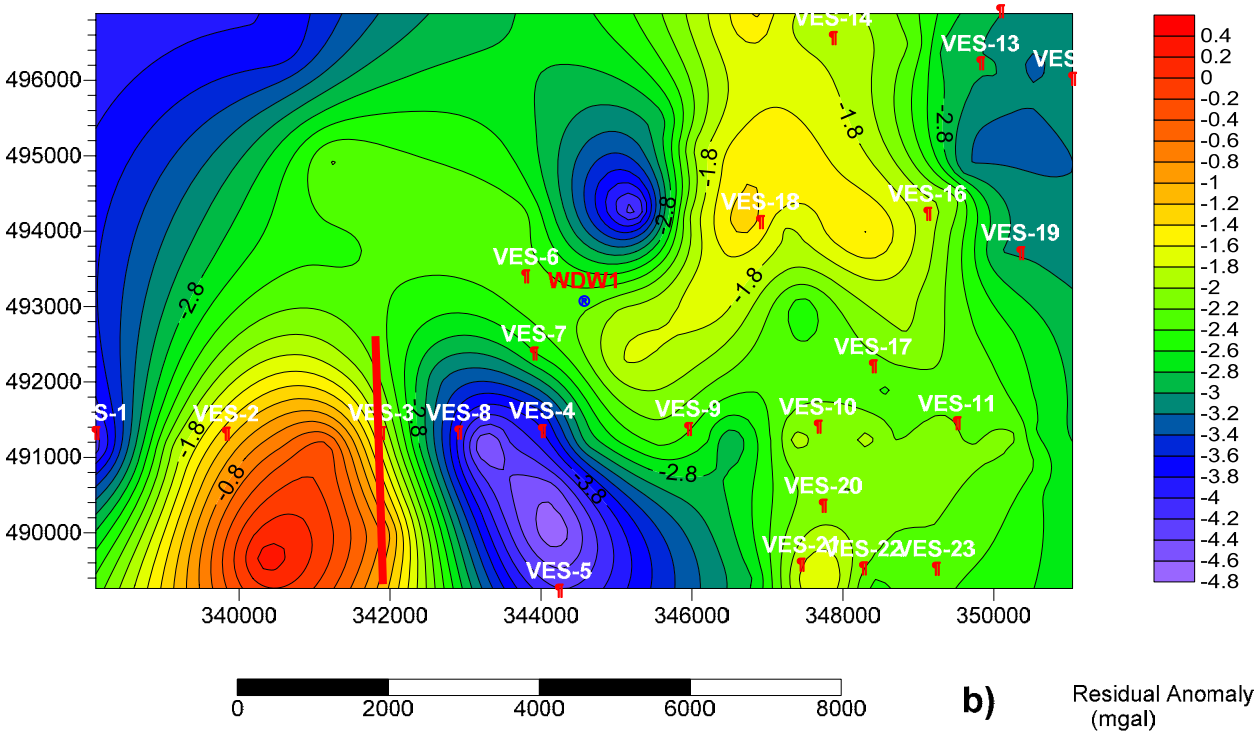

Figure 4.12(b) second degree residual anomaly

Zone II

The very low apparent resistivity zone with apparent resistivity value (0-150 ohm-m) in the central, eastern, south west and north east part of the Figure4.1 is covered by quaternary vesicular basalts. The apparent resistivity of this area decrease as the depth increase (Figure4.4). This is also shown in pseudodepth section survey line one and survey line six which crosses the central part of the study area . As one can see from pseudodepth section of survey Line One and Line six, the apparent resistivity value decrease beneath Line one VES-4 and Line sixVES-4.

The gravity profile along this survey Line shows that the second degree residual gravity anomaly value decreases from Line six VES-7 towards Line 6 VES-4. Similarly the Bouguer anomaly and first degree residual gravity anomaly value decreases from Line 6 VES7 toward Line 6 VES-4 and attain their minimum value near VES-5.

Zone III

The transition zone between zone I (high apparent resistivity zone) and zone II (low apparent resistivity zone) has a resistivity value ranging from (200-250) ohm-m covers the Western part of Figure 4.12(a). The North West and north east part of this zone has got large apparent resistivity value for current electrode of spacing AB/2=1000m (Figure 4.12a). Low apparent resistivity value was observed in southern part of (Figure 4.12a).

Similarly the western part of (Figure 4.12b) is defined by second degree residual gravity map as a transition zone or structure. Therefore, they are most probably related with fault or structure.

4.4 Quantitative interpretation

Quantitative interpretations of Geophysical data were done by modeling the resistivity and gravity survey results along selected profiles. The results of resistivity modeling were presented as a geoelectric sections whereas the gravity modeling were presented as a graph showing the match between the modeled and residual anomaly in the top part and modeled subsurface in the lower part of the model. The elevation of each layer rather than depth was used during the construction of geoelectric sections. These results were used to determine the depth to the aquifer and identify the different degree of weathered and fractured lithologic units as well as depth to the basement along profiles.

4.4.1 Geo-electric Sections

The final result from one dimensional inversion of VES data along two survey lines (Line-1 and 6) were used to construct the geoelectric sections in order to identify the distribution of different Lithologic units in the vertical direction. The software which were used for the inversion of the VES data were ResixIP and Win Resist whereas the plotting was carried out by using AutoCAD and later surfure9 software. The lithologic log from test borehole that is lying on these profiles was used to fix the thickness of each layer by grouping lithologic units by their type and degree

of weathering and fracturing. The pseudodepth sections along these survey lines were examined to see the relative resistivity variations when preparing geoelectric sections.

4.4.1.1 Geo-electric section along Line one (VES1 to VES-11)

The geoelectric section of Line one (Figure 4.13) was constructed from the model parameters of VES points data found along Line-1(V1-V11). The borehole WDBH1 (OWWDS,.2008) located around L1-V4 was used to constrain (fix) depth for L1-V4 and later parameterize the resistivity values and depths of the other VES points using this value. Table 4.1 shows the lithologic log of WDBH1 which was used to fix the depth and type of layers when L1-V4 was modeled. The geoelectric cross-section (Figure 4.13) indicates the shallow subsurface lithologic units in the study area which are represented by six major geoelectric units .The six major geoelectric units have relative resistivity in accordance with the following patterns, $\rho_1 < \rho_2 < \rho_3 > \rho_4 < \rho_5 < \rho_6$ with resistive value ρ_1 (1.5-64)0hm-m, ρ_2 (150-300), ρ_3 (180-680), ρ_4 (55-110), ρ_5 (130-170) and ρ_6 (750-1460). The resistivity value of the two upper parts $\rho 1$ (1.5-64)0hm-m and ρ_2 (150-300)ohm-m are correlated with silt clay soil with basalt and resistive fractured and slightly weathered dry basalt respectively.

Table 4.1 Lithologic log of WDBH1

Lithology	Depth(m) from the surface
Silt clay soil weathered basalt	0-30
Resistive fractured &slightly weathered dry basalt	30-65
Moderately fractured& slightly weathered vesicular basalt	65-110
Moderately fractured &weathered basalt	110-137
Highly weathered &fractured basalt	137-168
Fresh Basement (granitoid)	171-

The third resistivity layer ρ_3 (180-680) ohm-m which is overlaid by resistive fractured and slightly weathered dry basalt and under lain by highly weathered & fractured basalt has a wide range of resistive value and it is characterized by moderately fractured and slightly weathered

vesicular basalt. There are two inferred structure i.e fault beneath VES-2 and between VES-9 and VES-10, which may be act as a conduit for water flow.

The fourth resistivity layer ρ_4 (55-110) ohm-m which is sandwiched between two highly resistive layers is characterized by highly weathered and fractured basalt is expected to be a good source of ground water or a possible aquifer zone .

The fifth resistivity layer ρ_5 (130-170) ohm-m which is found beneath VES1 and between VES-10 and VES-11 is characterized by moderately fractured and weathered possible saturated basalt.

The sixth resistivity layer ρ_6 (750-1460) 0hm-m.is correlated with fresh basement (Granitoid)

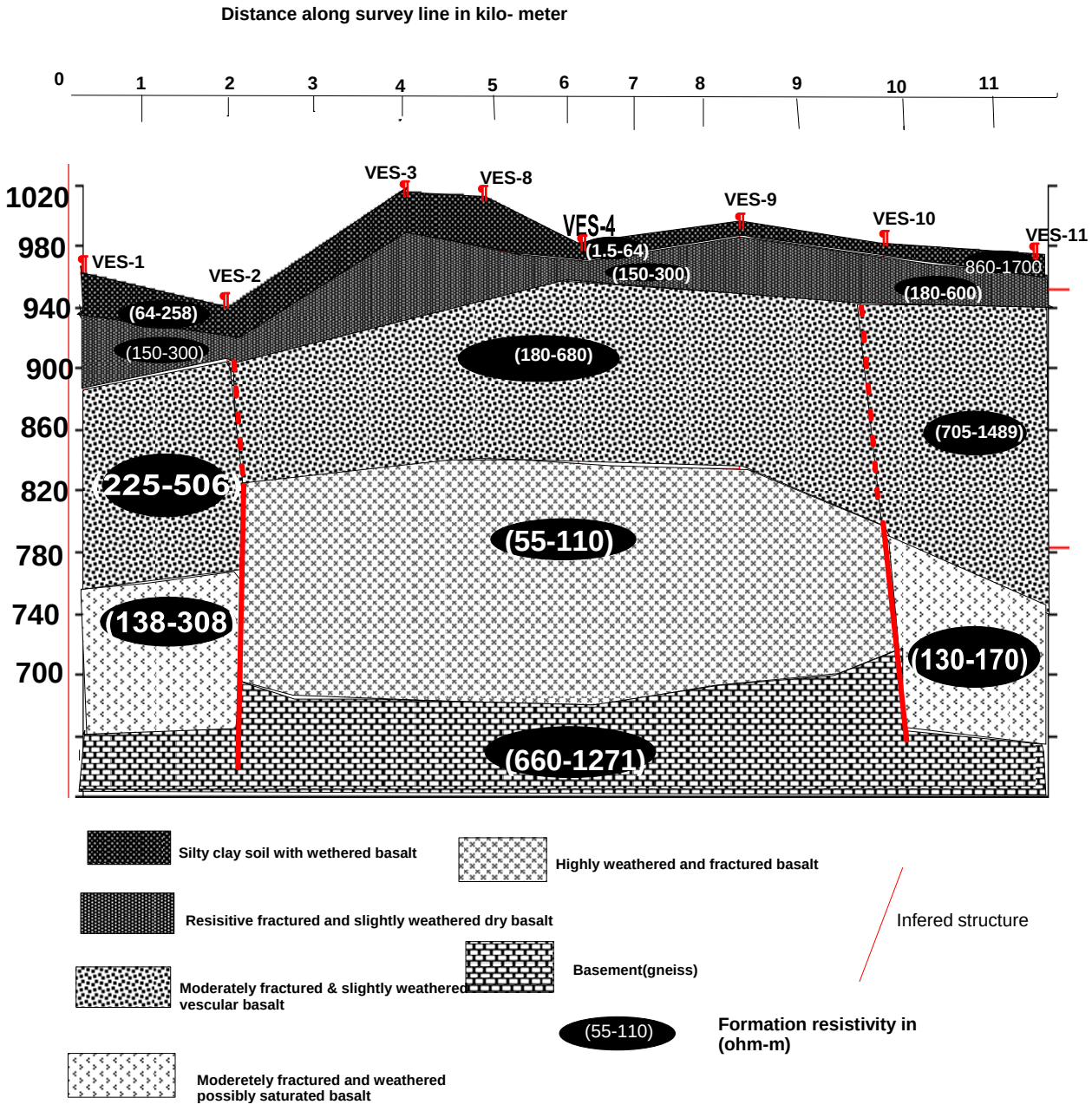

Figure 4.13 Geoelectric section along survey line one

4.4.1.2 Geo-electric section along Line six (VES7 to VES-5)

The geo-electric section of Line six (Figure4.14) was constructed from model parameter of VES point data along Line six (ves-7 to ves-5). The resistivity parameters found from modeling of each VES point data were used to prepare geoelectric section shown below in (Figure 4.14). The geoelectric section (Figure 4.14) shows that the shallow subsurface lithologic units found along line six which are represented by seven geo electric sections. The seven geoelectric units have a relative resistivity in accordance with the following patterns, $\rho_1 < \rho_2 < \rho_3 > \rho_4 < \rho_5 > \rho_6 < \rho_7$ with resistivity values ρ_1 (2-30) ohm-m, ρ_2 (60-220) ohm-m, ρ_3 (540-870) ohm-m, ρ_4 (4-46)0hm-m, ρ_5 (950-1150) ohm-m, ρ_6 (16-55) ohm-m, ρ_7 (70-130) ohm-m.

The first geoelectric layer ρ_1 (2-30) ohm-m correlated with basaltic flow with soil intercalation .The second geoelectric layer ρ_2 (60-220) ohm-m is correlated with highly weathered basalt . The third geoelectric layer ρ_3 (540-870) ohm-m which has a large coverage area is correlated with slightly weathered too massive basalt. The fourth geoelectric layer ρ_4 (4-46)0hm-m which is low resistivity zone and which is also a possible aquifer zone is correlated with extremely weathered , fractured possibly saturated basalt is surrounded by two fault line which may acts a conduit for ground water flow . The fifth geoelectric layer ρ_5 (950-1150) ohm-m which is relatively high resistivity zone is correlated with massive basalts. The sixth geoelectric layer ρ_6 (16-55) ohm-m which is relatively law in resistivity is also correlated with extremely weathered, fractured possibly saturated basalt. This layer is the same with layer ρ_4 (4-46)0hm-m except it is vertically as well as horizontally displaced from the position of layer ρ_4. This geoelectric layer is also a possible aquifer zone, and a good potential layer for ground water extraction. The seventh geoelectric layer ρ_7 (70-130) ohm-m is also relatively law in resistivity value and it may act as a good aquifer zone. This layer is correlated with highly weathered and fractured massive basalt.

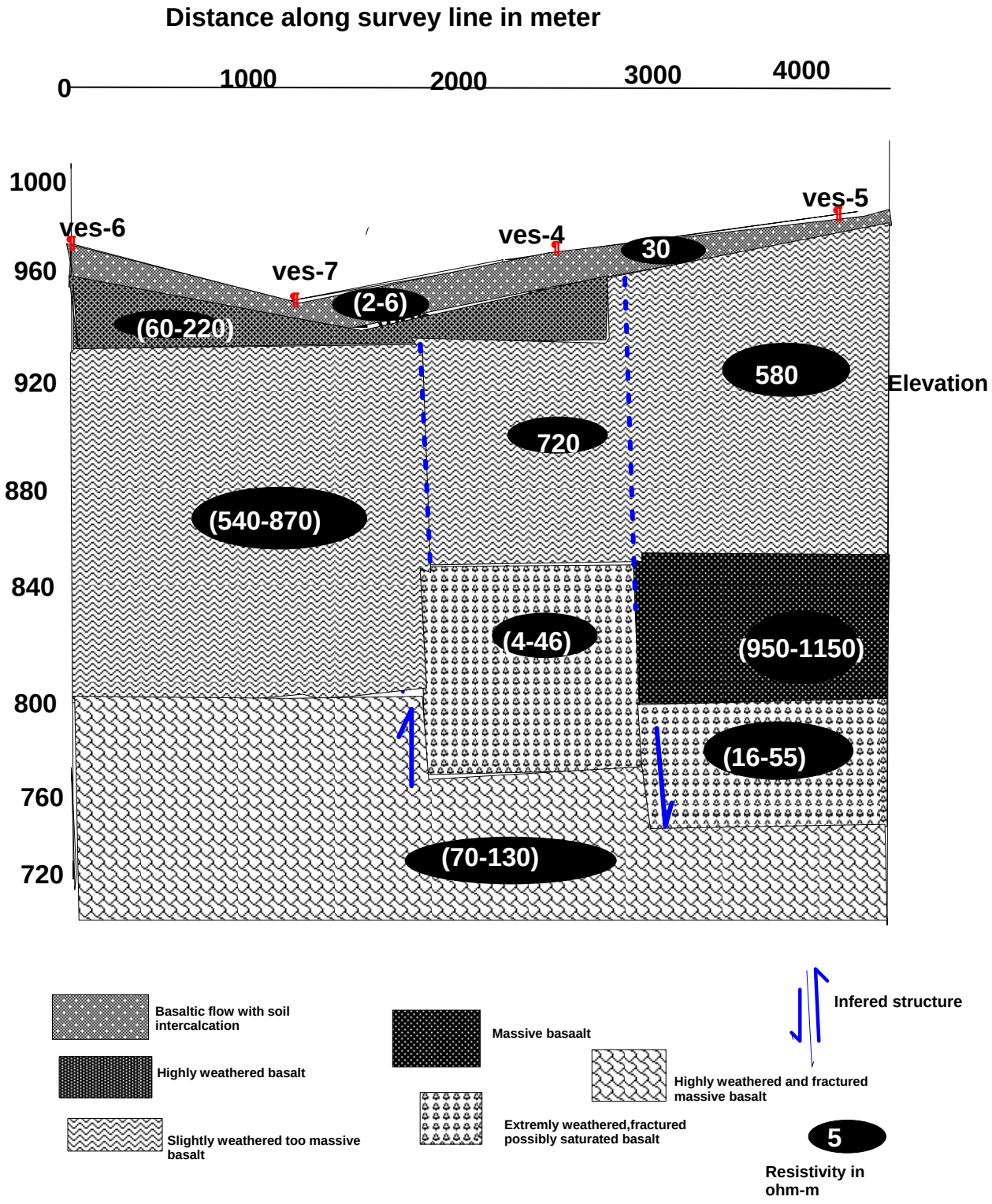

Figure 4.14 Geoelectric section along survey line six

4.4.2 Gravity Modeled section

Gravity modeling is usually the final step in gravity interpretation and involves trying to determine the density, depth and geometry of one or more subsurface bodies (Mickus, K., 2003). In this work, second degree polynomial surface fitting residual gravity anomaly data was used and the density contrast between the body of interest and the surrounding material was determined along one profile by using forward modeling of 2.5D bodies. The lithologic unit and depth constraints for modeling were taken from test borehole data and geoelectric sections and where as the density ranges of these rocks were taken from published density values (Telford et al 1990). Several trials and successive improvements were conducted to get best fit between the calculated and observed anomalies along the profile AA' (Figure 4.17). Since the gravity data has minimum separation of 300m and maximum separation of 1000m while the resistivity data has minimum separation of 1km and maximum separation of 2km, it is used to define clearly the causes of change in residual gravity anomaly observed in the qualitative maps. Unlike the resistivity method, the gravity data is not only caused by masses directly underneath but also by those found near of far away from the observation points. Moreover, the gravity measurement points are densely packed than the VES points with smaller sampling interval. Because of these, it has a great potential to model the subsurface horizontally in continuous way if appropriate constraint is laid on the vertical direction

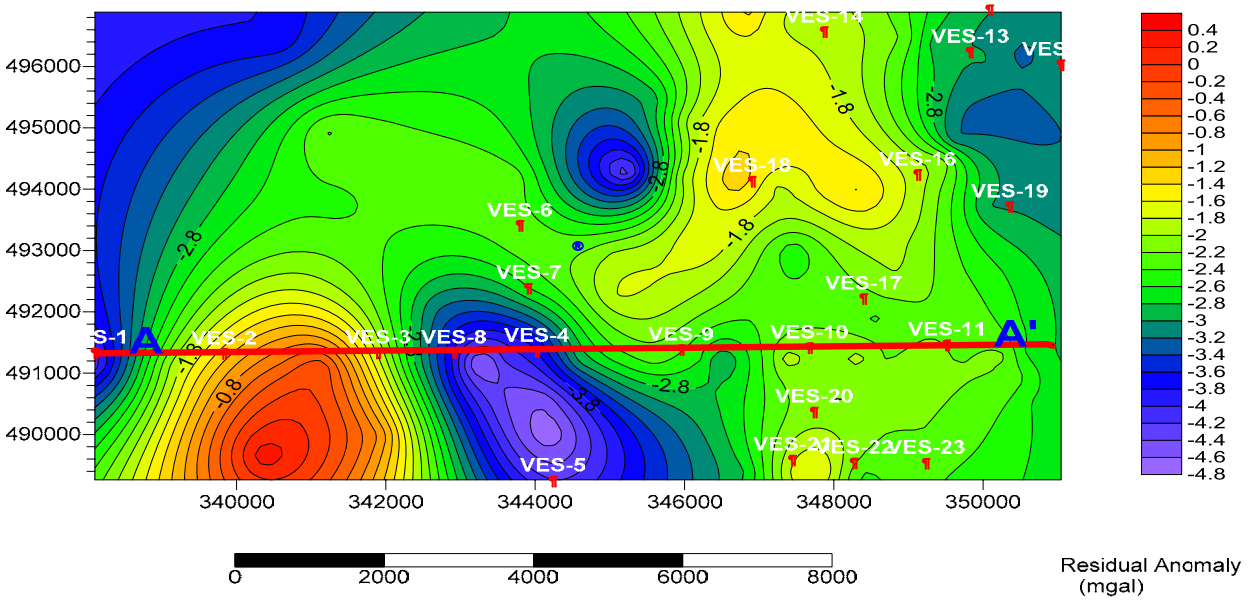

Figure 4.15 Modeled gravity profile from second degree residual gravity anomaly map along profile AA'

4.4.2.1 Gravity Modeled section along profile AA'

The gravity modeled section along AA' (Figure 4.16) was produced from the gridded second degree residual gravity anomaly data. The modeled profile is oriented in the west-east direction with a total length of 14km. It includes the resistivity survey Line one with additional length to the west and east. The densities and thickens of the lithologic units data from borehole and which were identified in the geo-electric section of Line One are used to constrain the gravity model parameter. The initial values of densities of these lithologic units were taken from literature (Telford et al 1990) and the values were freely adjusted to fit the gravity data based on their degree of weathering, fracturing type and depth of burial but within the range of densities taken from literature.

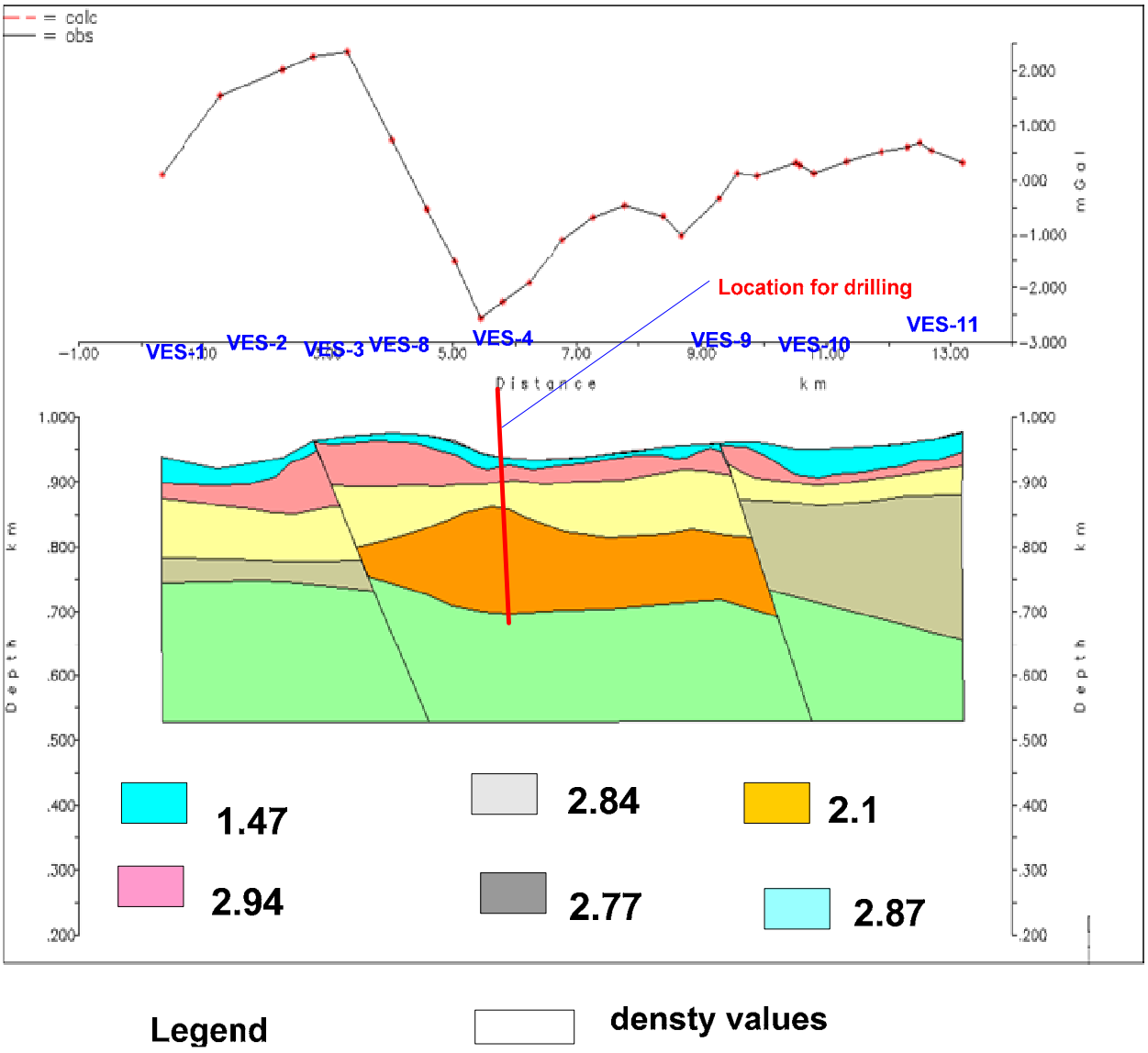

Figure 4.16 Gravity Modeled section along profile AA'

The modeling was performed by fitting the observed data with the calculated one by varying the geometry (depth and shape) on those places where we didn't have VES measurements. Where ever, we had VES measurements, depth of burial of lithologic units were fixed to VES result and minimum adjustments were made to those depth. After several trials, the model shown in Figure 4.16 which consists of different layers was obtained. Among these layers, the basement shown at the bottom has higher thickens with density contrast value of 0.2g/cm^3. The depth to the basement along this profile varies from west to east within 200m-330m rang.

The first layer which is silty clay soil with weathered basalt having density contrast of-1.2gm/cm^3. This layer is a little bit thicker at the west and east corner and thinner in the middle part. The modeled gravity section of the first layer has similar structure or clearly visible by the geoelectric section modeled along survey line one.

The second layer which is indicated in the Figure 4.16 is slightly fractured and slightly weathered dry basalt with relatively larger density contrast of about 0.27gm/cm^3. The pick value of residual anomaly near VES-3 is due to the relatively thicker and denser material beneath VES-3of the second layer. This layer is clearly visible in the modeled geoelectric section as layer two.

The third layer which is indicated in the Figure 4.16 is moderately fractured and slightly weathered vesicular basalt having density contrast of 0.17gm/cm^3. This layer is thicker at the west corner of the profile and thinner at the eastern corner of the profile. The third layer is displaced downward at western part and displaced upward at eastern part from its original position due to the two fault line structures. This layer is also clearly visible in the modeled geoelectric section along line one.

The minimum residual gravity value beneath VES-4 is caused by the highly weathered and fractured basalt with probably clay formation which has low density value with density contrast of-0.57gm/cm^3. This layer is also clearly visible in the geo-electric section along profile one by low resistivity zone and it is a possible source of groundwater potential.

The fourth layer which is interrupted by layer of highly weathered and fractured basalt is identified as moderately fractured and slightly weathered vesicular basalt. This layer is observed in the western and eastern part of the profile.

The orientation of the two structural Line observed in geo-electric section of Line One are also shown in the gravity modeled section.

Table 4.2 Rock types and their density values used for modeling along profile AA'.

Rock type	Density range (g/cm^3)	Average density (g/cm^3)	Density value used for modeling(g/cm^3)
Silty clay soil	1.2-2.4	1.29	1.47
Resistive fractured and Slightly weathered dry basalt	2.7-3.3	2.99	2.94
Moderately fractured and slightly weathered vesicular basalt	2.7-3.3	2.99	2.84
Moderately fractured and weathered possibly saturated basalt	2.7-3.3	2.99	2.77
Highly weathered and fractured basalt with probably clay formation	2.7-3.3	2.99	2.1
Basement(Gneiss)	2.59-3.0	2.8	2.87

CHAPTER FIVE

CONCLUSION AND RECOMMENDATION

5.1 Conclusion

This work presented the results of integrated geophysical survey that was conducted in the Borena Zone of Oromia Regional State, Southern Ethiopia with the aim to investigate groundwater potential zones and map possible structures, which serves as a conduit for groundwater movement. A total of 21VES and 103 gravity measuring points were measured to gather data. The data were carefully processed and interpreted. The interpretations were made qualitatively as well as quantitatively to achieve the desired objectives.

The qualitative interpretation of the VES data were performed by preparing apparent resistivity plan maps and pseudodepth sections whereas the interpretation of the gravity data were made based on the second degree residual gravity profile plots and different gravity anomaly maps. The quantitative interpretations of VES data were made using geo-electric section along two selected profiles. Information from a borehole and one VES point that is taken very near to the borehole were used to parameterize the inversion result from VES data. The interpretation helped to identify different lithologic units. On the other hand, the quantitative interpretation of gravity data was performed by using forward modeling of the second degree residual gravity anomaly along one selected profiles. To constrain the gravity data vertical information from a borehole and a number of VES points is used. The main aim of the gravity survey was to map the basement topography, geological structures and different layers in areas where VES information was not available. Especial focus was given in the mapping of the basement undulation.

There is test borehole as a result of this work in the study area. The comparison of the geophysical interpretations with drilled borehole results shows that the results of the integrated geophysical survey are in a very good agreement with the borehole logging results. The

comparison of well yield with the geophysical survey results demonstrated the capacity of using resistivity (VES) and gravity surveys together for demarcating groundwater potential zones, especially in diverse geologic situation where we have different lithologic units such as the one in the current survey area.

From the results, discussions and interpretation made in this study, the following conclusions have been made:

1) The groundwater flows using structures and fractures of lithologic units to accumulate over the basement wherever the basement has bowl like shape or depression. Therefore, whenever fault lines, fractures and low basement topography are interpreted and accompanied by low resistivity values at higher depths, these places are identified as good groundwater potential zones. As a result of the above, the place under VES4 has been recommended because it has low basement topography and the lowest resistivity value at higher depth and hence identified as the most favorable place for drilling.

2) The geoelectric sections show that the area has six to seven main types of geoelectric layers which differ in different degree of weathering, level of fracturing, composition, thickens and depths of burial. These are correlated with quaternary vesicular basalts, gravel (with weathered and fractured vesicular basalts), massive basalt with scoria and basement (gneiss). In some places, the top layer is covered by silty clay soil or black cotton soil with very small thickness. The test drilling results also shows that layer that directly overlain the upper part of the basement is mostly weathered and fractured relative to the other layers and is good aquifers depending on the location relative to the structures and the shape of basement topography.

3) The gravity modeling along profile AA' revealed that the depth to the basement varies from 200m to 330m. The densities of the different layers namely Silty clay soil, slightly fractured and slightly weathered dry basalt, moderately fractured and slightly weathered vesicular basalt, moderately fractured and possibly saturated basalt, highly weathered and fractured basalt and basement with their densities values 1.47g/cm^3, 2.94g/cm^3,2.84g/cm^3,2.77g/cm^3 ,2.1g/cm^{3}and 2.87g/cm^3 respectively.

5.2 Recommendation

Based on the outcome of this study, the following are recommended.

1) The aquifer system of the area is controlled by the structural lines and the basement topography so that drilling is recommended to be done at places having low resistivity at large AB/2 separation, low basement topography as deducted from gravity survey and where the structural futures such as faults are encountering massive basalts or where they terminate. The following two boreholes are recommended for drilling in the following order. The first borehole is recommended near VES-4 of survey Line One and the second bore hole is recommended near VES-5 of survey Line six with UTM coordinates (343976, 490986, 960) and (344209, 488785, 976) respectively.

2) Additional Vertical Electrical sounding survey is recommended in the south west of the current survey area to examine the extension of low resistivity zones.

3) Similar detailed gravity survey outside of the area is recommended to know the extension of faults that are believed to serve as conduit for groundwater flow and to study the extension of the promising low gravity and low resistivity zone in the south west part of the area.

4) Detailed structural geological investigations are recommended to study the density and orientation of weak zones as well as their natures such as dip, strike and their extension.

5) Further regional hydrological and hydrogeological investigations are recommended to understand the basin, amount of precipitation and evaporation which are used to estimate the percolation of surface water to the ground water.

ANNEX

MODELED VES CURVES

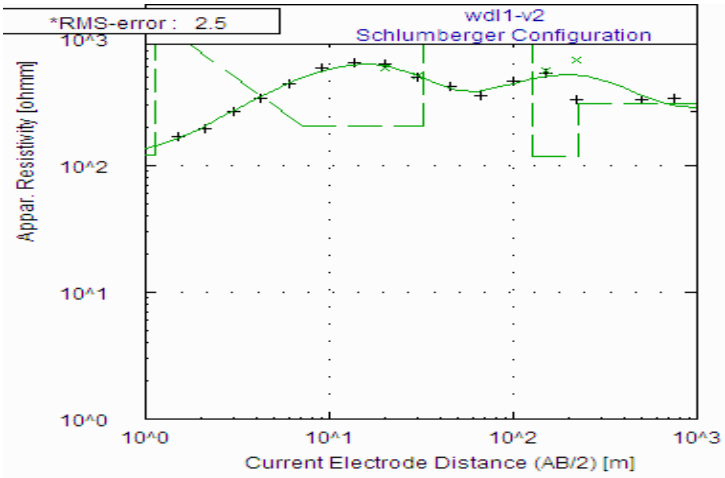

No	Res	Thick	Depth
1	122.0	1.1	1.1
2	1424.2	6.1	7.2
3	206.1	25.2	32.4
4	976.3	95.3	127.8
5	118.9	98.5	226.3
6	308.4	-.-	-.-

* RMS on smoothed data

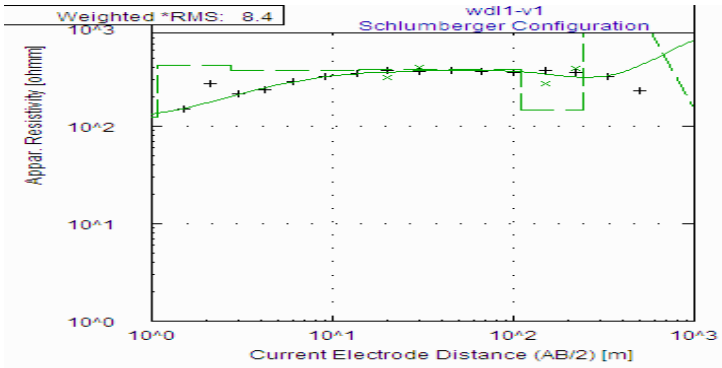

No	Res	Thick	Depth
1	122.7	1.1	1.1
2	421.4	1.7	2.7
3	374.9	11.2	14.0
4	381.9	97.2	111.2
5	147.1	131.7	242.9
6	16457.3	735.8	978.6
7	161.3	62.1	1040.7
8	0.4	-.-	-.-

* RMS on smoothed data

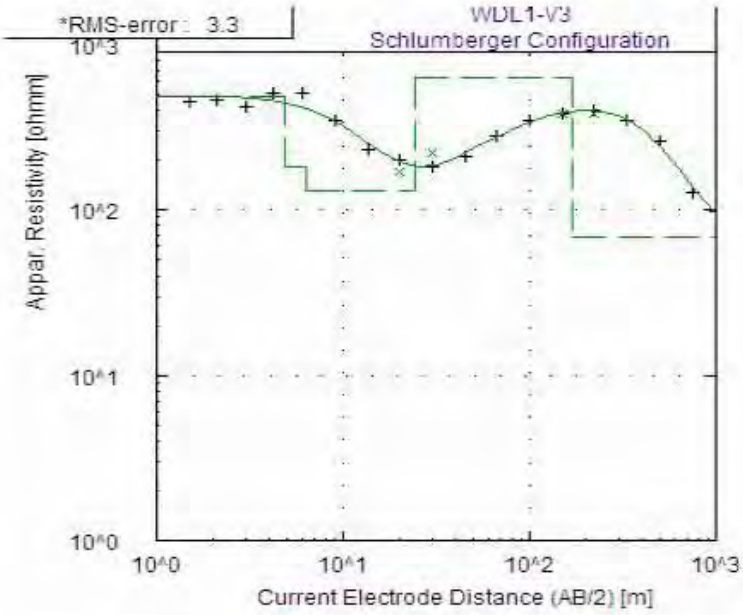

No	Res	Thick	Depth
1	489.9	4.9	4.9
2	181.0	1.4	6.3
3	130.7	17.9	24.2
4	628.0	143.7	167.9
5	67.7	-.-	-.-

* RMS on smoothed data

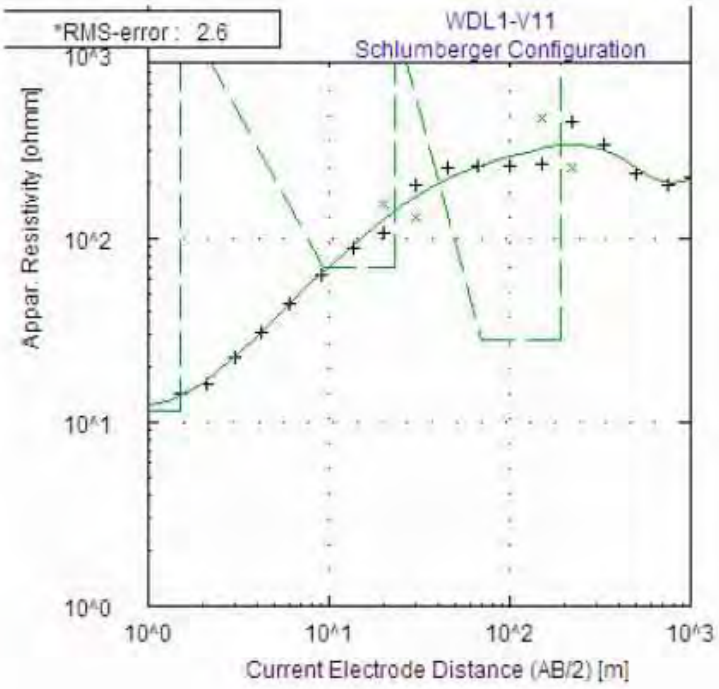

No	Res	Thick	Depth
1	11.4	1.5	1.5
2	1786.7	3.0	4.5
3	1198.1	4.7	9.3
4	69.2	13.9	23.1
5	1489.0	46.7	69.8
6	28.1	121.6	191.4
7	2475.6	-.-	-.-

* RMS on smoothed data

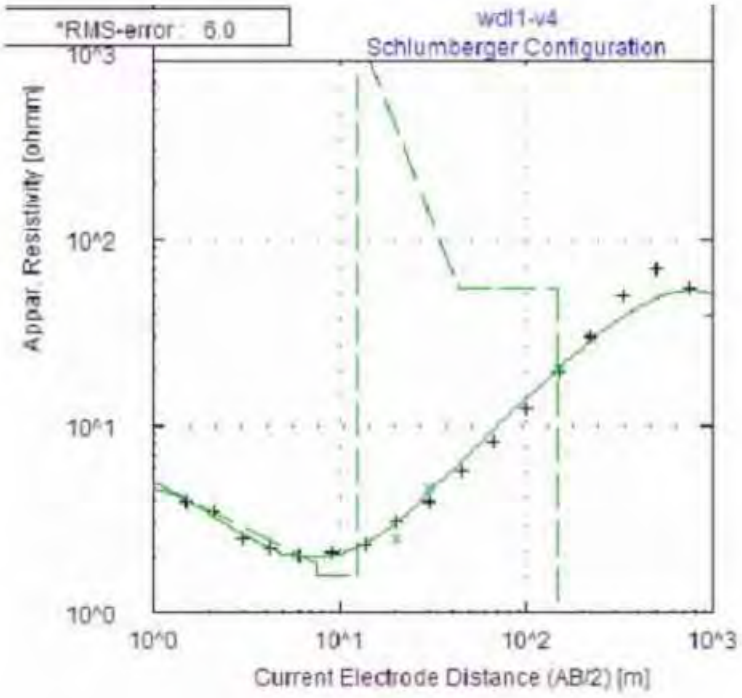

No	Res	Thick	Depth
1	5.1	0.9	0.9
2	1.8	6.6	7.6
3	1.6	4.7	12.3
4	1406.8	30.5	42.8
5	55.3	30.1	72.9
6	54.8	74.6	147.5
7	0.1	--	--

* RMS on smoothed data

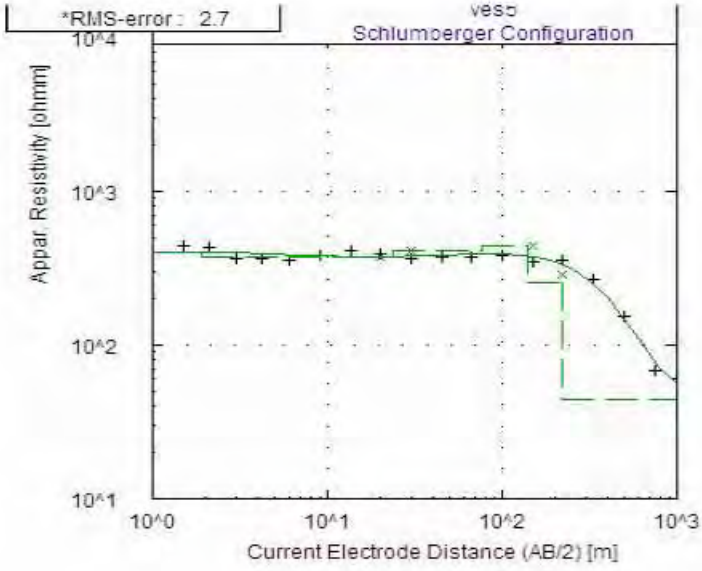

No	Res	Thick	Depth
1	406.3	1.9	1.9
2	373.0	21.6	23.5
3	407.5	52.6	76.1
4	437.2	64.6	140.7
5	255.6	77.8	218.5
6	43.8	--	--

* RMS on smoothed data

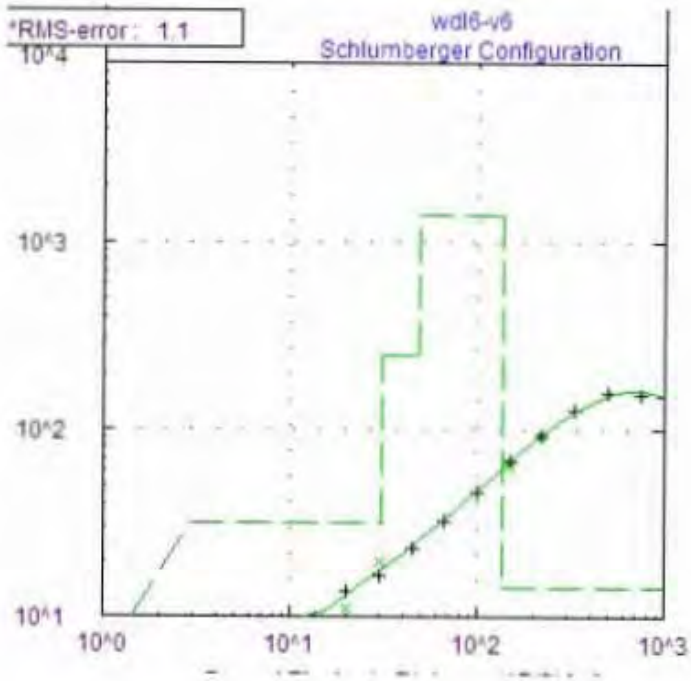

No	Res	Thick	Depth
1	5.5	1.0	1.0
2	2.2	1.9	2.9
3	31.3	27.7	30.6
4	250.9	18.4	49.0
5	1408.9	87.0	136.0
6	14.3	--	--

* RMS on smoothed data

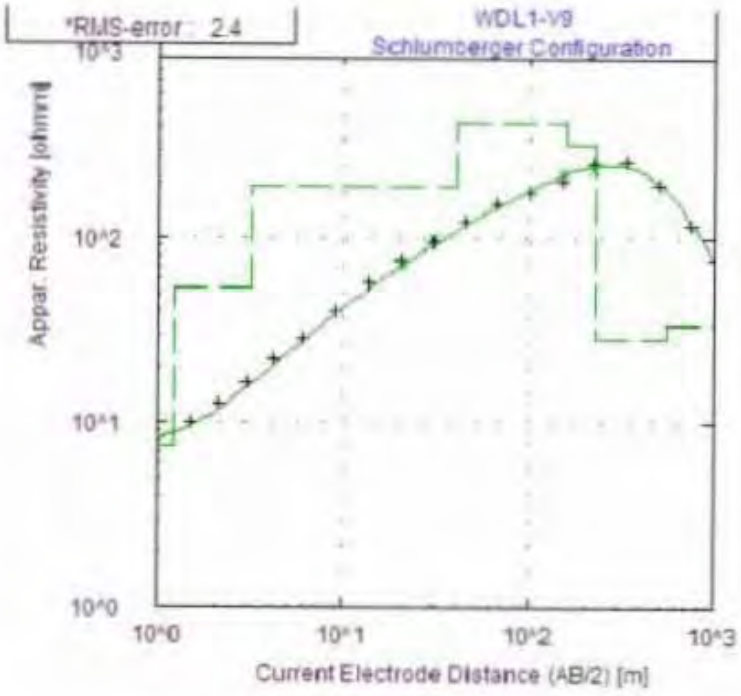

No	Res	Thick	Depth
1	7.4	1.2	1.2
2	53.5	1.9	3.1
3	189.3	37.5	40.6
4	420.9	118.8	159.4
5	325.4	68.9	228.3
6	29.0	320.3	548.6
7	33.9	--	--

* RMS on smoothed data

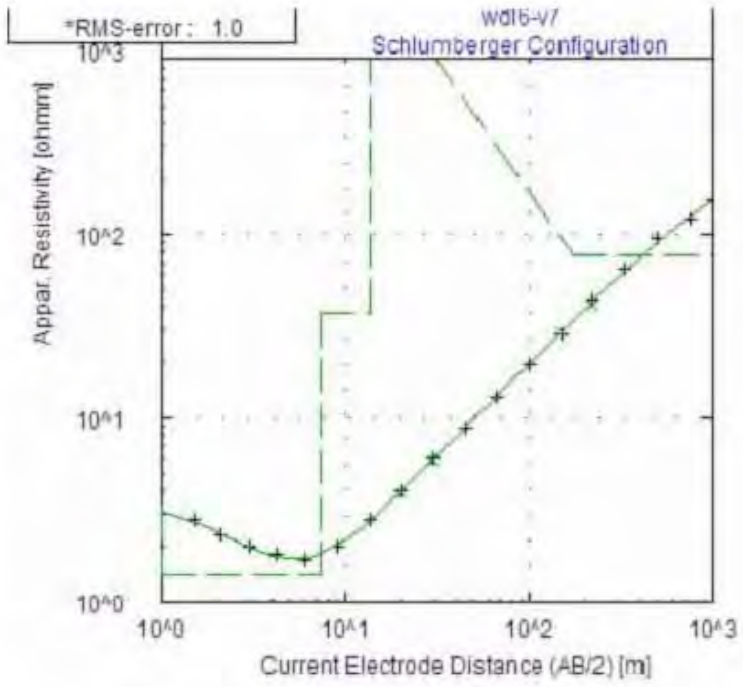

No	Res	Thick	Depth
1	3.3	1.0	1.0
2	1.4	6.4	7.4
3	37.4	6.4	13.8
4	2895.4	158.0	171.7
5	76.5	-.-	-.-

* RMS on smoothed data

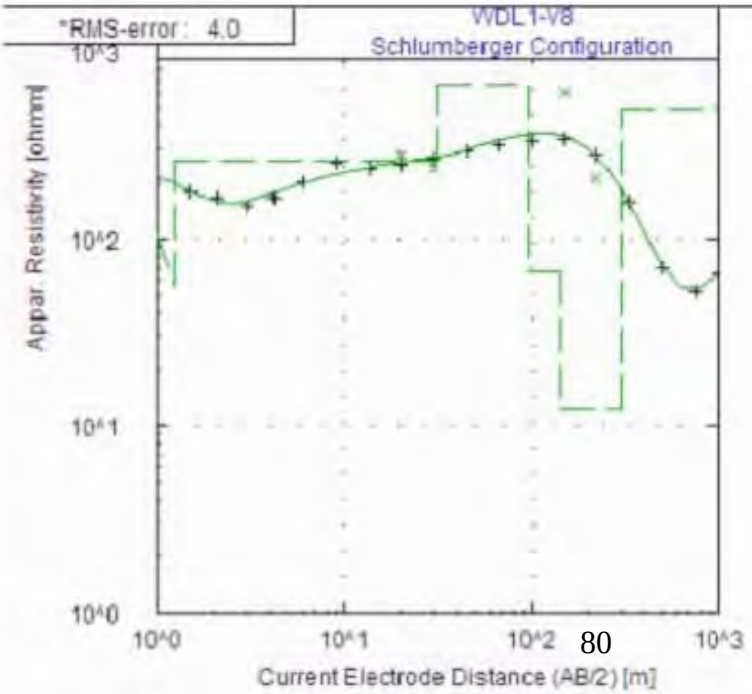

No	Res	Thick	Depth
1	258.8	0.7	0.7
2	56.6	0.5	1.2
3	263.9	30.6	31.8
4	671.3	64.4	96.2
5	66.8	46.8	143.0
6	12.4	158.1	301.1
7	487.8	-.-	-.-

* RMS on smoothed data

REFERENCES

.**Banerjee, B., and Gupta, S.P.D., 1997;** Gravitational attraction of rectangular parallepipe: Geophysics, vol.42, No.5, pp1053-1055

Becker, M., 1984; Analyses on hochpraezisen Schweremessungen. Dissertation, Deutsche Geodaetische Kommission, Reihe C, Nr. 294, Muenchen, Germany**.**

Belete, Y., Abaire, B., Asefaw, B., Tigabe, M., Shiferaw, D., Belachew, M., Adege, N., Mulachew, A. and Abdela, M., 2000; Hydrogeological, Geophysical and Engineering geological investigation of yabello map sheet (NB 37-14). Ministry of Mine and Energy, Ethiopian Institute of Geological Surveys, Hydrogeology, Engineering geology and Geothermal department, Addis Ababa, Ethiopia**.**

Blakely, J.R., 1996; Potential theory in gravity and magnetic applications. Cambridge University press, Cambridge, UK. Pp 43-63,128-154.

Dobrin, M.B. and Savit, C. H., 1988; Introduction to geophysical prospecting, fourth edition. McGraw-Hill, New York, USA .Pp498-613,750-837.

Elias Lewi., 1997; Modeling and inversion of High precision Gravity data. Dissertation ,Deutsche Geodaetische Kommission, Reihe C Nr.471, Muenchen ,Germany

Fetter, C.W., 2001; Applied Hydrogeology,4th Edition. Prentice-Hall, Inc. London, UK. Pp120.

Gibson, P.J.and George, D.M., 2003; Environmental applications of geophysical surveying techniques. Nova Science Publishers, Inc. New York, USA .Pp45-49,137-177.

Hussein B., 1999 The geology, structure and geochemistry of crystalline rocks of the Moyale area, south Ethiopia; Implication for the tectogenesis of Precambrian basement, Band50, Tubinger, Germany

Kazmin V.,1970 Geological Map of Yabello area ,unpublished report ,United Nations-Ethiopia Mineral Survey.

Kazmin, V., 1972; Geology of Ethiopia, Explanatory notes to geological map of Ethiopia. Ethiopian Institute of Geological surveys, Addis Ababa, Ethiopia.

Kirsch, R., 2006; Groundwater Geophysics. A Tool for Hydrogeology. Springer-Verlag Berlin Heidelberg, Germany.

Mickus, K., 2003; Gravity method: environmental and engineering applications. Department of Geosciences, Southwest Missouri State University, Springfield, MO 65804; Pp1-10.

Mulugeta Chanie.,2010; Application of integrated geophysical techniques to map groundwater potential zones and geological structures at Gelchet Area, Borena Zone, South Ethiopia (unpublished)**.** Department of Earth Sciences, Addis Ababa University, Addis Ababa, Ethiopia.

Morelli, C., C. Gantar, T. Honkasalo, R. K. McConnell, J.G. Tanner, B. Szabo, U. Uotila, C.T. Whalen, 1974; The International Standardization Net 1971 9IGSN71). I.U.G.G.-I.A.G.-Publ. Spec. No. 4, Paris

Moritz, H., 1984; Geodetic Reference System 1980. In: C.C. Tscherning (ed), The Geodesist's Handbook 1984 – Bull.Geod. 58, 388-398

NAGY D. 1966; the gravitational attraction of a right rectangular prism. geophysics

OWWDSE, 2008; Detailed reconnaissance geological study of Borena zone, Borena groundwater study project geology report. Oromia water works, Design and supervision enterprises, Addis Ababa, Ethiopia. Pp1-50.

Parasnis, D.S., 1962: principle of applied geophysics, 3rd edition. Chapman and hall, London, England. Pp 59-96, 98-129.

Reynolds, J.M., 1997; An Introduction to Applied and Environmental Geophysics. John Wiley and Sons limited, England, UK. Pp 29-116,415-522.

Robinson, E.S., and Caruh, C., 1988; Basic exploration geophysics. John Wiley and Sons Limited, New York, USA. Pp 221-324.

Sultan, A. Mekhemer, M. Santos, M. and Abdi Alla, M., 2009: Geophysical measurements for subsurface mapping and groundwater exploration at the central part of the Sinia peninsula, Egypt. The Arabian journal for science and Engineering, volume 34, Number1a. Pp103-118.

Telford, W.M., Geldart, L.P. and Sheriff, R.E., 1990; Applied Geophysics, 2nd Edition. Cambridge University Press, Cambridge, UK. Pp 6-48,522-562.

Tesfaye Demissie,, **2007;** The geology of yabello map sheet *(*NB 37-14).Geological survey of Ethiopia, Regional Geology and Geochemistry department, Addis Ababa, Ethiopia

TORGE, W., 1989; Gravimetry, Walter de Gruyter and Co., Berlin, Germany

WSDP,2010; Federal Democratic Republic of Ethiopia Ministry of water Resources, Water Sector Development Program, Main report Volume II, Addis Ababa, Ethiopia Pp1-170

Declaration

This thesis is my original work and has not been presented for degrees in any other University and all sources of materials used for the thesis have been duly acknowledged.

Abdisa Kawo Koji Signature_____ Date_____

Dr.Elias Lewi (Advisor) Signature_____
Date_____

Dr.Tigistu Haile (Co-advisor) Signature_____
Date_____

OCTOBER, 2011

Addis Ababa